Synthesis of Isotopically Labeled Fe and S-alkylated Iron-Sulfur Clusters

by

Brittany Linn

B.S. Chemistry

Purdue University, 2021

SUBMITTED TO THE DEPARTMENT OF CHEMISTRY IN PARTIAL FULFILLMENT OF THE REQUIREMENTS FOR THE DEGREE OF

MASTER OF SCIENCE IN CHEMISTRY

AT THE

MASSACHUSETTS INSTITUTE OF TECHNOLOGY

May 2024

Authored by:

_____

Brittany Linn

Department of Chemistry

May 12, 2024

Certified by:

_____

Daniel L. M. Suess

Associate Professor of Chemistry

Thesis Supervisor

Accepted by:

_____

Adam Willard

Professor of Chemistry

Graduate Officer

SIGNATURE PAGE

Authored by:

_____

Brittany Linn
Department of Chemistry
May 12, 2024

Certified by:

_____

Daniel L. M. Suess
Associate Professor of Chemistry
Thesis Supervisor

Accepted by:

_____

Adam Willard
Professor of Chemistry
Graduate Officer

Synthesis of Isotopically Labeled Fe and S-alkylated Iron-Sulfur Clusters

by

Brittany Linn

Submitted to the Department of Chemistry
on May 12, 2024 in Partial Fulfillment of the
Requirements for the Degree of
Master of Science in Chemistry

ABSTRACT

Radical *S*-adenosylmethionine (SAM) enzymes (RS enzymes) use a 3:1 site-differentiated $[Fe_4S_4]^+$ cluster to reductively cleave the SAM cofactor and generate a 5'-deoxyadenosyl radical intermediate (5'-dAdo•) that regio- and stereospecifically abstracts an H-atom from the target substrate. It has been proposed that 5'-dAdo• binds to the unique Fe site before abstracting an H-atom from the substrate. However, due to the transient nature of captured reaction intermediates, their precise structures have yet to be fully elucidated and, therefore, their role in the mechanism of RS enzymes remains unclear. Our group has established reliable methods of synthesizing alkylated $[Fe_4S_4]$ clusters that can serve as models of organometallic intermediates in RS enzyme catalysis. These clusters are competent for radical release and, upon oxidation, undergo an alkyl migration process to yield S-alkylated clusters. A cluster species containing a unique alkylated Fe site with a coordination number greater than four is likely generated in these processes, although a stable cluster of this type has yet to isolated and crystallographically characterized. This work reports the synthesis of α-^{2}H and α-^{13}C isotopically labeled Fe and S ethyl ligated $[Fe_4S_4]$ clusters to determine their electron-nuclear hyperfine parameters by ENDOR spectroscopy. These parameters will aid in identification of alkylated $[Fe_4S_4]$ cluster intermediates generated in biological studies. Additionally, in an attempt to synthesize an $[Fe_4S_4]^{+3}$ cluster with a five coordinate, Fe-alkylated site, a series of benzyl and phenyl ligated clusters were prepared and analyzed by NMR and EPR spectroscopies.

Thesis Supervisor: Daniel L. M. Suess

Title: Associate Professor of Chemistry

TABLE OF CONTENTS

LIST OF FIGURES

Chapter 1

Introduction

1.1 Introduction

Organisms from all kingdoms of life possess radical *S*-adenosyl methionine (SAM) enzymes—the largest known protein superfamily—to catalyze a diverse set of challenging radical reactions, initiated by H-atom abstraction of substrate C–H bonds.[1] For example, radical SAM enzymes are known to catalyze more than 70 different chemical reactions that are important for protein and RNA modifications, DNA repair, antibiotic synthesis, and more. Responsible for their reactivity is an $[Fe_4S_4]^+$ cluster that contains an unique Fe site that is coordinated by the amino and carboxylate moieties of SAM and provides the electron required for the homolytic cleavage of the S–C5' sulfonium bond of SAM to generate a 5'-deoxyadenosyl radical intermediate (5'-dAdo•). While it was initially thought that the 5'-dAdo• was 'tamed' by van der Waals contact with its reaction partner to minimize its motion in the protein active site,[2] EPR and ENDOR spectroscopic studies of a trapped intermediate suggest a very different mechanism in which an organometallic species (dubbed Ω) is generated by the formation of a covalent bond between the unique Fe site of the cluster and the 5'C of 5'-dAdo• to make a formally $[Fe_4S_4]^{3+}$ cluster containing an alkylated six-coordinate Fe site (**Figure 1.1**).[3] Formation of an Fe–C5' bond in RS enzymes is analogous to the Co–C5' bond in adenosylcobalamin enzymes and could provide a means to control 5'-dAdo• and curtail H-atom abstraction of unintended C–H bonds.[3, 4] Due to the transient nature of Ω, its precise structure and role in the RS enzyme reaction pathway have yet to be determined by other experimental methods, which has sparked some controversy in the field. For example, generation of Ω also requires significant protein rearrangements that are hard to reconcile with the precise positioning of the substrate in the active site pocket.[2] Furthermore, some computational studies

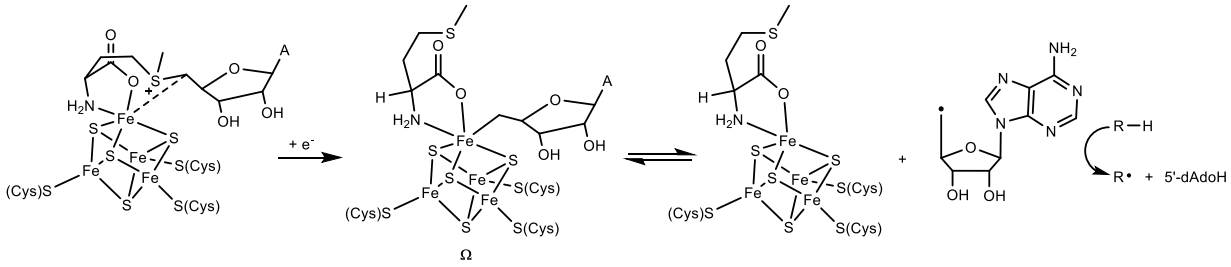

Figure 1.1 Proposed mechanism of 5'-dAdo• generation in radical SAM enzymes.[3]

have suggested that Ω could be a shunt product in certain RS enzymes, [5] or that the hyperfine coupling values observed for Ω are most consistent with a near-attack conformer of SAM with a constrained distance of 3.0 Å between the unique Fe of the cluster and the S atom of SAM.[6]

To contribute to the mechanistic understanding of RS enzymes, our lab has established reliable methods for synthesizing alkylated $[Fe_4S_4]$ clusters that serve as fully characterizable models (**Figure 1.2**). We have used these complexes to determine how strong-field, electron-donating alkyl ligands affect the structure and valence electron distribution of $[Fe_4S_4]$ clusters and the reactivity of the Fe–alkyl bond.[7-10] For example, we have determined that the addition of pyridine to alkylated $[Fe_4S_4]^{2+}$ clusters, results in the release of primary carbon radicals via reversible Fe–alkyl bond homolysis.[9] The likely mechanism of radical release proceeds through an intermediate containing a five-coordinate Fe site that is transiently bound by both the alkyl ligand and the N-

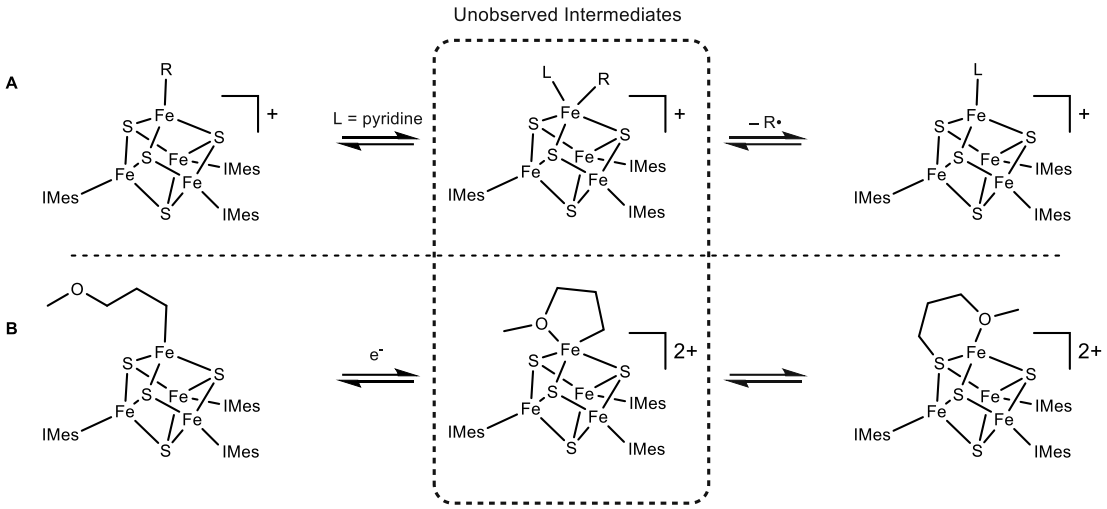

Figure 1.2 A. Reaction of alkylated $[Fe_4S_4]^{2+}$ clusters with pyridine, demonstrating the formation of an intermediate with a five coordinate Fe site.[9] **B**. Possible mechanism of alkyl group migration proceeding through an intermediate species with a five coordinate Fe site.[10]

atom of the pyridine donor, and we therefore affirmed that the strength of the Fe–alkyl bond in the higher coordinate intermediate is significantly weakened by higher coordination number at the unique Fe site. This evidence supports that radical SAM enzymes may use coordination number to modify the Fe–C bond strength to control the rate of homolysis and the selectivity of H-atom abstraction.[9] However, the instability of five coordinate intermediate species has prevented its characterization; therefore, we have yet to determine the extent to which higher coordination number at the unique Fe site weakens the Fe–C bond.

1.2 References

(1) Broderick, J. B.; Duffus, B. R.; Duschene, K. S.; Shepard, E. M. Radical *S*-Adenosylmethionine Enzymes. *Chem. Rev.* **2014**, 114, 4229-4317

(2) Horitani, M.; Byer, A. S.; Shisler, K. A.; Chandra, T.; Broderick, J. B.; Hoffman, B. M. Why Nature Uses Radical SAM Enzymes so Widely: Electron Nuclear Double Resonance Studies of Lysine 2,3-Aminomutase Show the 5′-DAdo• "Free Radical" Is Never Free. *J. Am. Chem. Soc.* **2015**, *137* (22), 7111–7121.

(3) Horitani, M.; Shisler, K.; Broderick, W. E.; Hutcheson, R. U.; Duschene, K. S.; Marts, A. R.; Hoffman, B. M.; Broderick, J. B. Radical SAM Catalysis via an Organometallic Intermediate with an Fe–[5′-C]-Deoxyadenosyl Bond. *Science* **2016**, *352* (6287), 822–825.

(4) Brown, A. C.; Suess, D. L. M. Reversible Formation of Alkyl Radicals at [Fe4S4] Clusters and Its Implications for Selectivity in Radical SAM Enzymes. J. Am. Chem. Soc. 2020, 142 (33), 14240–14248.

(5) Zhao, C.; Li, Y.; Wang, C.; Chen, H. Mechanistic Dichotomy in the Activation of SAM by Radical SAM Enzymes: QM/MM Modeling Deciphers the Determinant. ACS Catal. 2020, 10 (22), 13245–13250.

(6) Donnan, P. H.; Mansoorabadi, S. O. Broken-Symmetry Density Functional Theory Analysis of the Ω Intermediate in Radical S-Adenosyl-l-Methionine Enzymes: Evidence for a Near-Attack Conformer over an Organometallic Species. J. Am. Chem. Soc. 2022, 144 (8), 3381–3385.

(7) Ye, M.; Thompson, N. B.; Brown, A. C.; Suess, D. L. M. A Synthetic Model of Enzymatic [Fe_4S_4]–Alkyl Intermediates. *J. Am. Chem. Soc.* **2019**, *141* (34), 13330–13335.

(8) McSkimming, A.; Sridharan, A.; Thompson, N. B.; Müller, P.; Suess, D. L. M. An $[Fe_4S_4]^{3+}$ – Alkyl Cluster Stabilized by an Expanded Scorpionate Ligand. *J. Am. Chem. Soc.* **2020**, *142* (33), 14314–14323.

(9) Brown, A. C.; Suess, D. L. M. Reversible Formation of Alkyl Radicals at [Fe_4S_4] Clusters and Its Implications for Selectivity in Radical SAM Enzymes. *J. Am. Chem. Soc.* **2020**, *142* (33), 14240–14248.

(10) Ye, M.; Brown, A. C.; Suess, D. L. M. Reversible Alkyl-Group Migration between Iron and Sulfur in [Fe4S4] Clusters. *J. Am. Chem. Soc.* **2022**, *144* (29), 13184–13195.

Chapter 2. Synthesis of Isotopically Labeled Ethyl-Ligated $[Fe_4S_4]^{n+}$ Clusters

2.1 Background

Radical *S*-adenosylmethionine (SAM) enzymes are ubiquitous in nature and use a protein-bound 3:1 site-differentiated $[Fe_4S_4]^{+}$ cluster to reductively cleave the SAM cofactor, generating a 5'-deoxyadenosyl radical intermediate (5'-dAdo•) that regio- and stereospecifically abstracts an H-atom from an otherwise unactivated C–H bond and thereby initiates a wide array of different radical reactions.[1] In all cases, it is thought that 5'-dAdo• binds to the unique Fe site before abstracting an H-atom from the substrate. Interestingly, the substrate radical can then attack a different, auxiliary Fe–S cluster; in some cases, this occurs at S, and in others it is not clear if it's Fe or S (**Figure 2.1**).[2-7]

Isolation of these species in biological systems is challenging because of their short lifetimes. Rapid freeze-quench (RFQ) electron paramagnetic resonance (EPR) and electron nuclear double-resonance (ENDOR) spectroscopies have been used to trap and analyze transiently stable paramagnetic species. While these techniques provide information that is related to the structure and reactivity of biological molecules, EPR and ENDOR spectroscopies cannot definitively characterize these species. Synthetic models—which can be fully characterized—are needed for comparison.

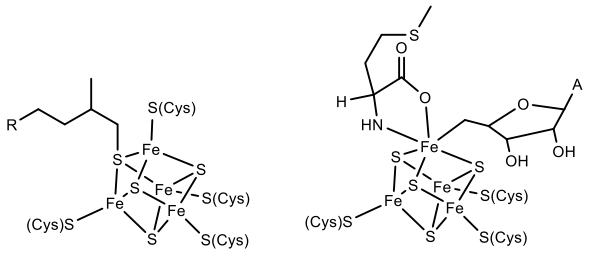

Figure 2.1 Examples of proposed S-alkylated (left) and Fe-alkylated (right) $[Fe_4S_4]$ cluster intermediates in enzymatic reactions.

Synthetic S-alkylated $[Fe_4S_4]^{n+}$ clusters had not been accessed until recently when our group discovered the occurrence of alkyl group migration upon oxidation of synthetic Fe-alkylated $[Fe_4S_4]^{+1}$ clusters to the $[Fe_4S_4]^{3+}$ state in the presence of a coordinating group, which thereby produces an S-alkylated species.[8] In the absence of an available coordination partner (e.g., an oxygen atom donor), alkyl migration does not occur and Fe-alkylated $[Fe_4S_4]^{3+}$ are obtained.

A series of isotopically labeled, S-alkylated $[Fe_4S_4]^{3+}$ clusters were synthesized to determine their electron-nuclear hyperfine parameters by ENDOR spectroscopy in collaboration with Professor Brian M. Hoffman's laboratory at Northwestern University. Because hyperfine tensors are a reflection of (i) the extent of delocalization of the unpaired electron spin onto a given nucleus and (ii) the interaction between the magnetic moments of the electron and nuclear spins in a molecule, hyperfine values can identify the nuclei within the first coordination sphere of a paramagnetic complex and, thereby, provide information on its bonding, geometry, and structure. EPR linewidths of Fe-S proteins are often too broad to resolve hyperfine coupling, therefore advanced ENDOR techniques are implemented to extract this information. Measuring the hyperfine coupling of synthetic S-alkylated $[Fe_4S_4]^{3+}$ clusters will not only enable the identification of S-alkylated intermediates observed in enzymatic studies but will also set a new benchmark for computational studies predicting the reaction pathways involving such intermediates.

2.2 Results and Discussion

The scalable 3:1 site differentiated cluster $(IMes)_3Fe_4S_4Cl$ (IMes = 1,3-dimesitylimidazol-2-ylidene)[9] was the chosen precursor to prepare the series of ethyl alkylated $[Fe_4S_4]^{n+}$ clusters for this investigation. Unlike previous alkyl groups our group has used, halo-ethane is commercially available in both its α-^{2}H and α-^{13}C labeled forms, enabling determination of hyperfine parameters by ENDOR. Cluster **1** is cleanly produced by addition of 1.05 equivalents of a 0.1 M solution of ethyl magnesium halide in tetrahydrofuran to a solution of $(IMes)_3Fe_4S_4Cl$ in a mixture of diethyl ether and tetrahydrofuran (1:1) followed by addition of 1,4-dioxane and filtration through celite to remove magnesium salts. Cluster **1** is oxidized to the $[Fe_4S_4]^{3+}$ state by addition of two equivalents of ferrocenium (Fc^+) in a mixture of difluorobenzene and tetrahydrofuran (9:1) at -35 °C (**Figure 2.2**). Immediately upon the addition of Fc^+, an aliquot of the reaction mixture (~ 80 µL) is loaded into a Q-band EPR tube and glassed in liquid nitrogen to capture the thermally unstable S-alkylated cluster, **2**. These procedures were repeated to prepare the -$C^2H_2CH_3$ and -$^{13}CH_2CH_3$ isologues of this complex in the $[Fe_4S_4]^+$ and formally $[Fe_4S_4]^{3+}$ states.

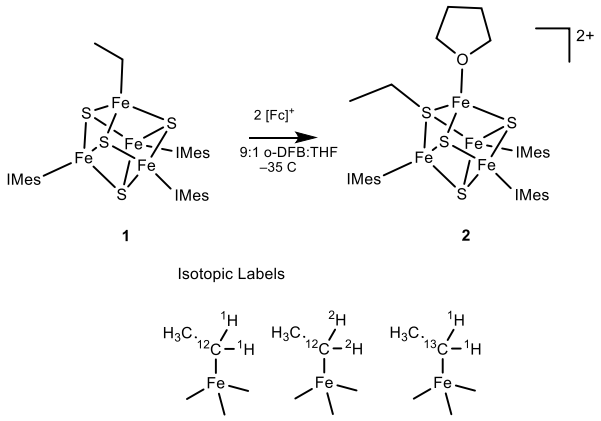

Figure 2.2 Preparation of ^{1}H, ^{2}H and ^{13}C isologues of the S-alkylated $[(IMes)_3Fe_4S_4CH_2CH_3]^{2+}$ cluster.

Although a complete analysis of these samples is still underway, we have found that, as expected, the *g* values of **1** (g = 2.12, 1.95, 1.93; g_{avg} = 2.00) are nearly identical to $(IMes)_3Fe_4S_4(CH_2CH_2CH_2OMe)$, a related Fe-alkylated $[Fe_4S_4]^+$ cluster previously synthesized by our group, (g = 2.12, 1.96, 1.93; g_{avg} = 2.00)[8]. Further, ^{1}H ENDOR analysis of **1** revealed a coupling of ~18 MHz for the α-1H protons of the alkyl group. For the S-alkylated cluster, **2**, it was difficult to resolve the very small couplings of the ethyl protons from ^{1}H ENDOR experiments because of the relatively smaller amount of spin delocalized onto the bridging sulfides of the cluster compared to Fe atoms. Using pulsed ^{2}H ENDOR experiments to eliminate the background of unlabeled protons, an isotropic coupling of A ~ 0.5 MHz was preliminarily estimated for the S-alkylated species, corresponding to an analogous proton hyperfine value of 3 MHz. Additional ENDOR experiments are currently being conducted to determine the sign of this coupling as well as the full ^{1}H, ^{2}H and ^{13}C hyperfine values of these and other samples.

2.3 Summary and Conclusions

Synthetic models of proposed intermediates in enzymatic reactions, such as the radical chemistry performed by radical SAM enzymes, will aid in the identification of species trapped by RFQ and other techniques. Recently, S-alkylated $[Fe_4S_4]^{3+}$ clusters were discovered upon oxidation of synthetic Fe-alkylated $[Fe_4S_4]^+$ clusters and, therefore, a series of isotopically labeled, ethyl ligated clusters were synthesized to determine their electron-nuclear hyperfine parameters by ENDOR spectroscopy. Characterization of these clusters enables the identification of biological

intermediates and sets a benchmark for computational studies of these enzymes. Further investigation is ongoing to fully analyze the obtained data and elucidate the role of S-alkylated clusters in RS enzyme mechanisms.

2.4 Experimental

General Considerations. All reactions were performed using standard Schlenk techniques or in an LC Technologies inert-atmosphere glovebox under an atmosphere of dinitrogen. Glassware was dried in an oven at 160 °C prior to use. Molecular sieves (3 Å) and Celite were activated by heating to 300 °C overnight under vacuum prior to storage under an atmosphere of dinitrogen. Diethyl ether (Et_2O), toluene and pentane were degassed by sparging with argon, dried by passing through a column of activated alumina and stored under an atmosphere of dinitrogen over 3 Å molecular sieves. o-Difluorobenzene (o-DFB) was distilled from CaH_2, C_6D_6 was degassed by three freeze-pump-thaw cycles. Tetrahydrofuran (THF) was distilled from sodium/benzophenone and stored under an atmosphere of dinitrogen over 3 Å molecular sieves. C_6D_6 was degassed by three freeze-pump-thaw cycles and stored under an atmosphere of dinitrogen over 3 Å molecular sieves. Grignard reagents were prepared by addition of the alkyl halide to activated magnesium turnings in THF. [Fc][$BArF_4$] ([$BArF_4$] = [$B(3,5\text{-}(CF_3)_2Ph)_4$]) and $(IMes)_3Fe_4S_4Cl$ (IMes = 1,3-dimesitylimidazol-2-ylidene) were synthesized by reported procedures.[9,10] All other reagents were purchased from commercial suppliers and used without further purification/drying unless otherwise noted. NMR spectra were recorded on Bruker 400 and 500 MHz spectrometers. EPR spectra were recorded on a Bruker EMX spectrometer at 9.37 GHz as frozen glasses.

$(IMes)_3Fe_4S_4(CH_2CH_3)$

$(IMes)_3Fe_4S_4Cl$ (40mg, 31μmol) was dissolved in a 1:1 mixture of Et_2O and THF (2 mL) and cooled to -78 °C. A chilled solution of ethyl magnesium bromide (0.1 M, 0.3 mL, 33 μmol) was added dropwise. After 30 minutes of stirring at -78 °C, the mixture was diluted with Et_2O (8 mL) at room temperature. 1,4-Dioxane (1 mL) was added to the solution and stirred vigorously for 10 minutes. The solution was filtered through celite and the filtrate was reduced to dryness. The resulting precipitate was redissolved in Et_2O (8 mL) and 1,4-dioxane (1 mL) was added to the solution. After vigorous stirring for 30 minutes, the solution was filtered through celite and reduced to dryness. Recrystallization by diffusing pentane onto a Et_2O solution at -35 °C for 12 hours afforded the product as dark crystals. These procedures were repeated with isotopically labeled ethyl magnesium bromide to prepare the $-C^2H_2CH_3$ and $-^{13}CH_2CH_3$ isologues. Yield: 26.4 mg (66.3%). ^{1}H NMR (400 MHz, C_6D_6, 298 K): δ 256 (s, 2H, Fe$CH_2$$CH_3$), 43 (s, 3H, $FeCH_2CH_3$), 7.0 (s, 12H, IMes Ar*H*), 6.16 (s, 6H, backbone C*H*), 2.32 (s, 18H, Mes *p*-CH_3), 2.06 (s, 36H, IMes *o*-CH_3).

$[(IMes)_3Fe_4S_4(CH_2CH_3)][BAr^F]_2$ – S alkylated

$(IMes)_3Fe_4S_4(CH_2CH_3)$ (4.7 mg, 3.6 μmol) and [Fc][$BArF_4$] (7.6 mg, 7.3 μmol) were separately dissolved in an 8:1:1 mixture of o-DFB, Et_2O and toluene (1.8 mL total reaction volume) and cooled to -35 °C. The solution of [Fc][$BArF_4$] was added to the $(IMes)_3Fe_4S_4(CH_2CH_3)$ solution and immediately an aliquot of the reaction mixture (0.2 mL) was transferred into an X-band EPR tube and glassed in liquid nitrogen. Due to its thermal instability, this compound was made freshly for all experiments and analyzed at cryogenic temperatures.

2.5 References

(1) Broderick, J. B.; Duffus, B. R.; Duschene, K. S.; Shepard, E. M. Radical *S*-Adenosylmethionine Enzymes. *Chem. Rev.* **2014**, 114, 4229-4317

(2) Booker, S. J. Anaerobic Functionalization of Unactivated C—H bonds. *Curr. Opin. Chem. Bio.* **2009**, 13, 58-73

(3) Lanz, N. D., Pandelia, M. E.; Kakar, E. S.; Lee, K. H.; Kredb, C.; Booker, S. J. *Biochemistry*. **2014**, 53, 4557-4572

(4) McLaughlin, M. I.; Lanz, N. D.; Goldman, P. J.; Lee, K. H.; Booker, S. J.; Drennan, C. L. Crystallographic Snapshots of Sulfur Insertion by Lipoyl Synthase. *PNAS*. **2016**, 113, 9446-9450

(5) Cicchillo, R. M.; Booker, S. J. Mechanistic Investigations of Lipoic Acid Biosynthesis in *Escherichia coli*: Both Sulfur Atoms in Lipoic Acid are Contributed by the Same Lipoyl Synthase Polypeptide. *J. Am. Chem. Soc.* **2005**, 127, 9, 2860-2861

(6) Lanz, N. D.; Rectenwalk, J. M.; Wang, B.; Kakar, E. S.; Laremore, T. N.; Booker, S. J.; Silakov, A. Characterization of Radical Intermediate in Lipoyl Cofactor Biosynthesis. *J. Am. Chem. Soc.* **2015**, 137, 13216-13219

(7) Lloyd, C. T.; Iwig, D. F.; Wang, B.; Coosu, M.; William, W. M.; Boal, A. K.; Booker, Q. J. Discovery, Structure and Mechanism of a Tetraether Lipid Synthase. *Nature*. **2022**, 609, 197-203

(8) Ye, M.; Brown, A. C.; Suess, D. L. M. Reversible Alkyl-Group Migration between Iron and Sulfur in [Fe_4S_4] Clusters. *J. Am. Chem. Soc.* **2022**, *144* (29), 13184–13195.

(9) Brown, A. C.; Suess, D. L. M. Controlling Substrate Binding to [Fe_4S_4] Clusters through Remote Steric Effects. *Inorg. Chem.* **2019**, *58* (8), 5273–5280.

(10) Blechschmidt, D. R.; Lovstedt, A.; Kass, S. R. Metallocenium Lewis Acid Catalysis for Use in Friedel-Crafts Alkylation and Diels-Alder Reactions. *Organometallics*. **2022**, *41*(18), 2648-2655

2.6 Spectra

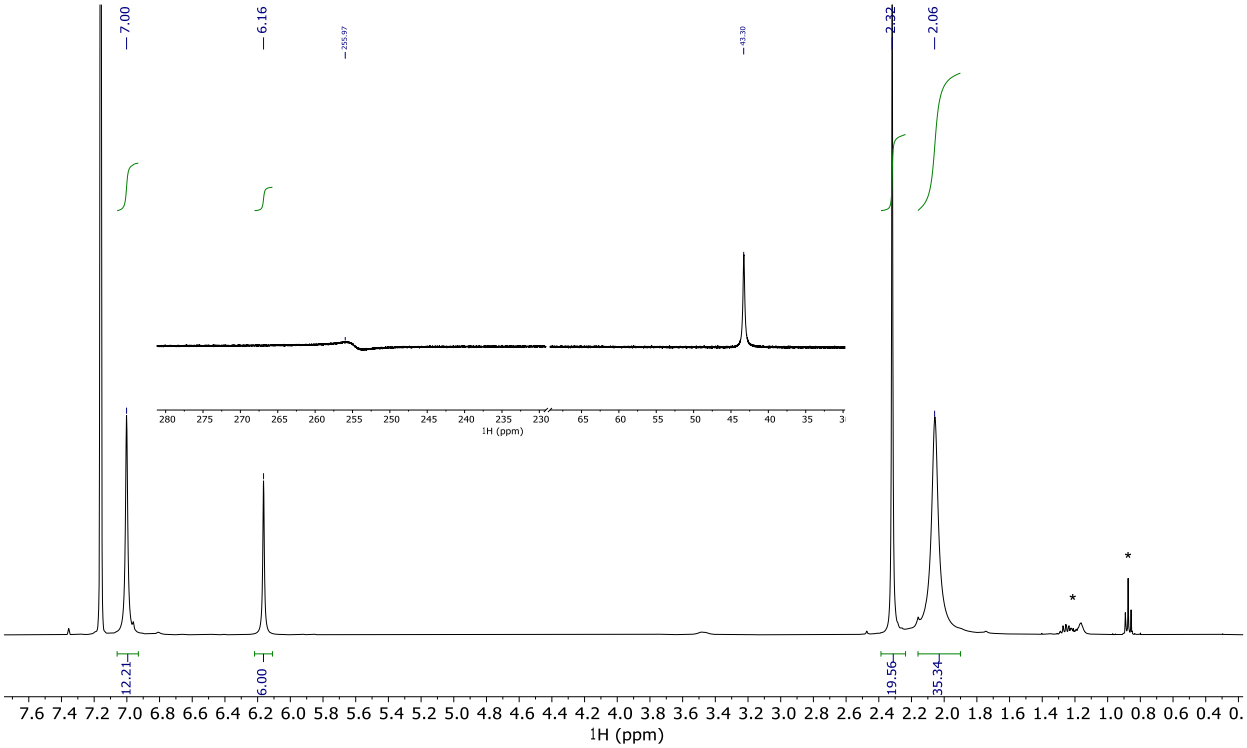

Figure S2.1. ^{1}H-NMR spectrum of $(IMes)_3Fe_4S_4CH_2CH_3$ in C_6D_6 (* pentane)

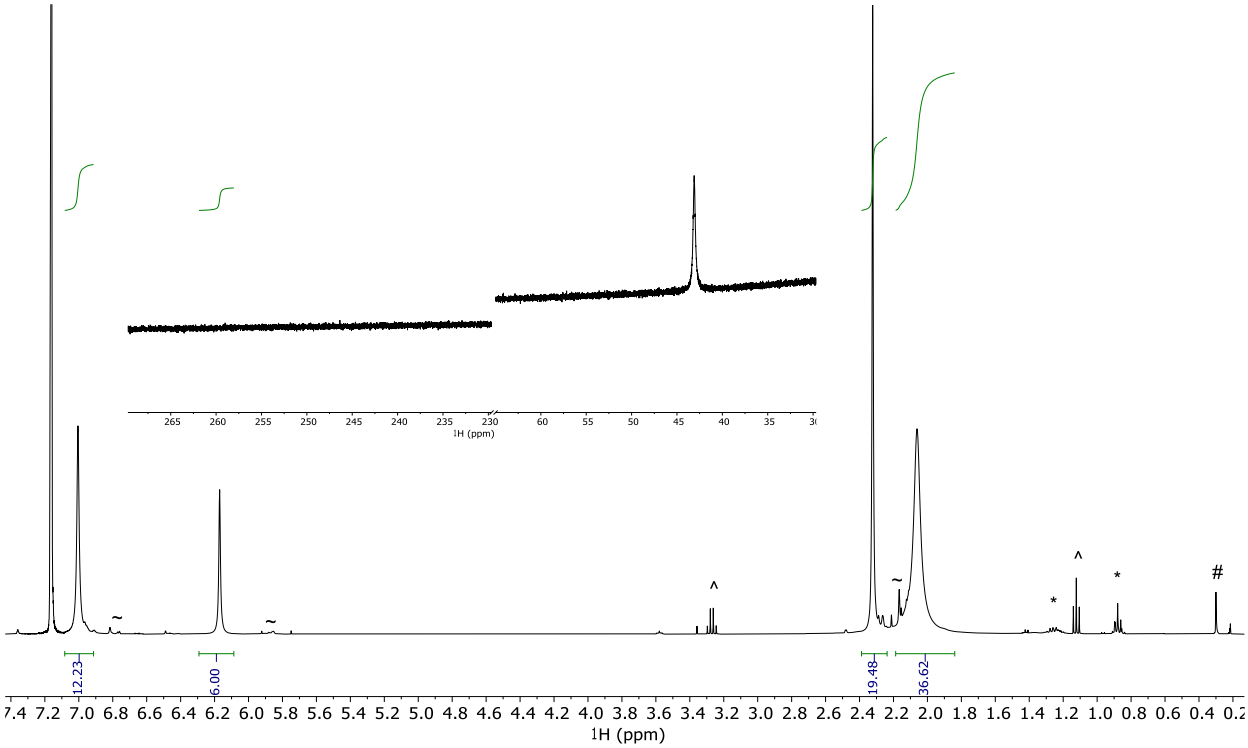

Figure S2.2. ^{1}H-NMR spectrum of $(IMes)_3Fe_4S_4C^2H_2CH_3$ in C_6D_6 (* pentane, ^ Et_2O, # grease, ~ unknown impurity)

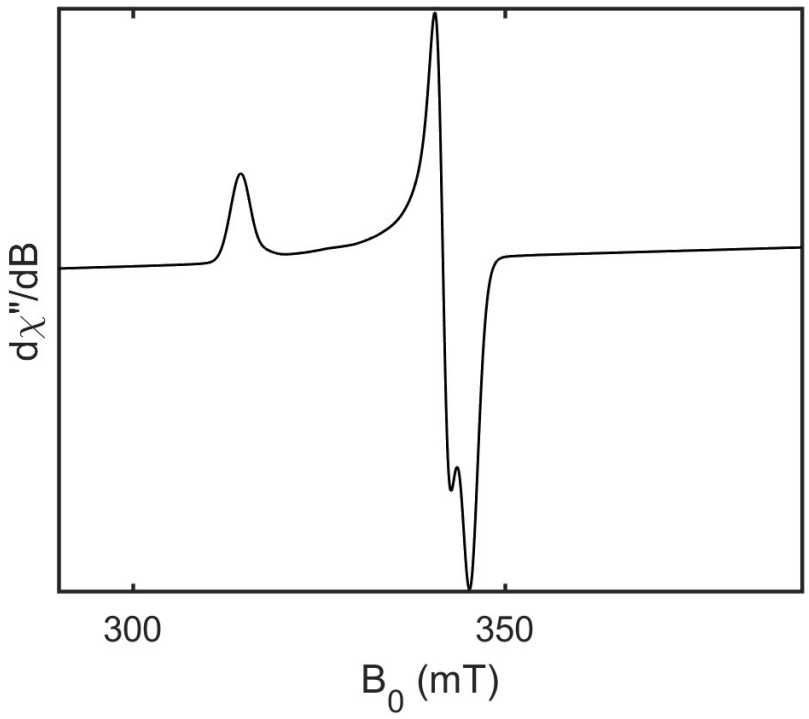

Figure S2.3. X-band EPR spectrum of $(IMes)_3Fe_4S_4CH_2CH_3$ (15K, 63 μW, g = [2.13, 1.96, 1.94])

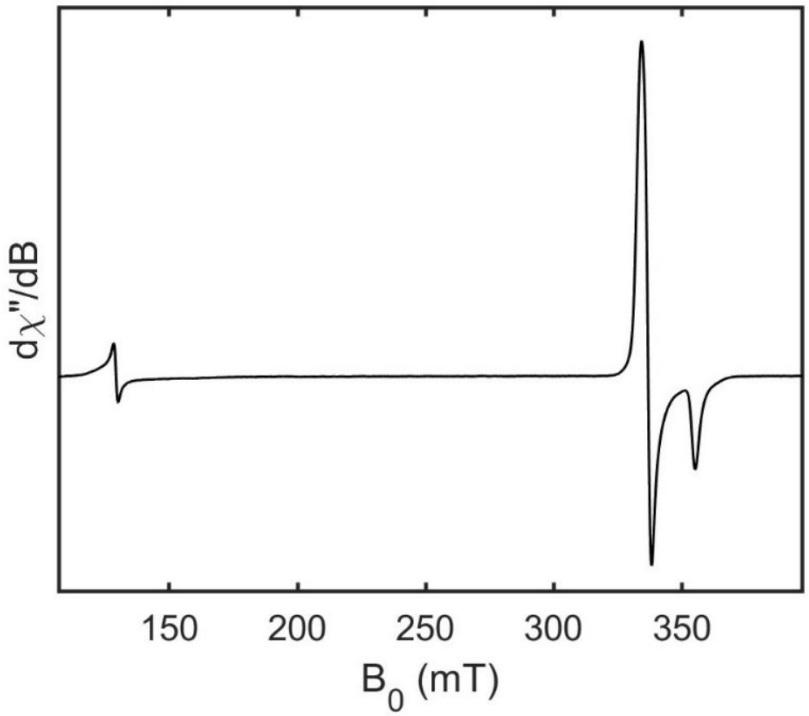

Figure S2.4. X-band EPR spectrum of $[(IMes)_3Fe_4S_4CH_2CH_3][BArF_4]_2$—S alkylated (15K, 63 μW, g = [1.99, 1.99, 1.88] for the S = 1/2 signal and g_{eff} = 5.19 for the S = 7/2 signal)

Chapter 3. Development of a Series of Benzyl and Phenyl Ligated $[Fe_4S_4]^{n+}$ Clusters

3.1 Background

To synthesize an $[Fe_4S_4]$ cluster containing a unique alkylated Fe site with a coordination number of five, our group hypothesized that alkyl groups containing an L-type donor atom (e.g., O, N, etc.) may bind the unique Fe site in a bidentate fashion (**Figure 3.1**).[1] In the $[Fe_4S_4]^{+1}$ core oxidation state in $(IMes)_3Fe_4S_4(CH_2CH_2CH_2OMe)$ (**1-MP**), the alkylated Fe site retains tetrahedral geometry, but, unexpectedly, oxidation to the $[Fe_4S_4]^{3+}$ state induces alkyl group migration to a nearby μ_3 sulfide, while a dative bond forms between the L-type donor atom of the ligand and the unique Fe site, as described in the preceding chapters. Like Fe–C bond homolysis,[2] alkyl group migration may involve a higher-coordinate intermediate, giving further credence to the highly reactive nature of alkylated Fe sites with a coordination number greater than four.

Isolation and characterization of an $[Fe_4S_4]$ cluster with a unique, penta- or hexa- coordinated alkylated Fe site would help elucidate the identity of Ω. Specifically, it's spectroscopic signature and electron-nuclear hyperfine parameters can be compared to those obtained for Ω to support the evidence that Ω contains an Fe–C bond.

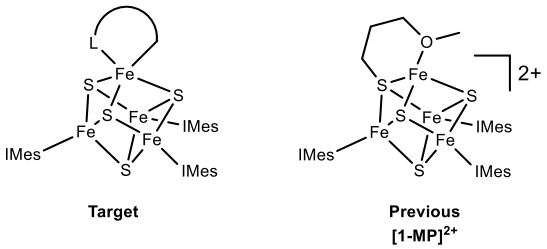

Figure 3.1 Target compound to model Ω (left) and previously isolated S-alkylated $[Fe_4S_4]^{3+}$ cluster (right).

To disfavor alkyl migration from Fe to S upon oxidation, we envisioned three different approaches (**Figure 3.2**). Firstly, we modified the ligand backbone of **1-MP** to a more rigid, benzyl backbone, which could experience ring strain upon migration to a cluster sulfide and, therefore, would instead remain coordinated to the unique Fe site. Secondly, a stronger Fe–C bond (e.g., between Fe and a sp^2 hybridized C atom instead of sp^3) was proposed to hinder aryl group migration because the homolysis product is unfavorable (if indeed the homolysis product is an intermediate in alkyl/aryl migration). Lastly, long chain alkyl ligands that form a 6-membered ring at Fe, may be more stable than those that form a 5-membered ring due to reduced ring strain. For example, if alkyl ligands intended to form a 6-membered ring at Fe migrate to a nearby cluster sulfide, a 7-membered ring would form, which may be less stable.

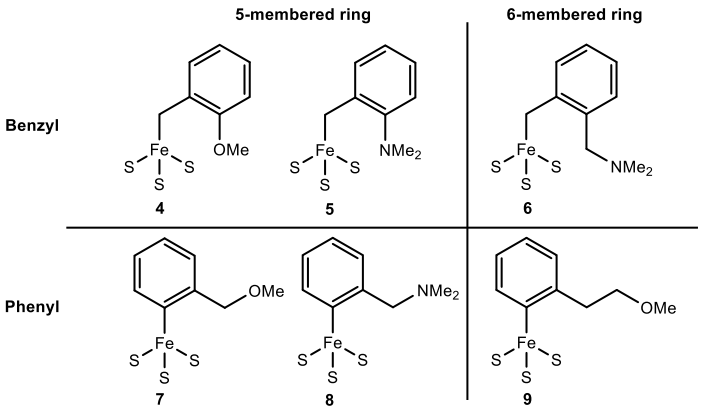

Figure 3.2 Ligand designs implementing the three approaches ((1) using an alkyl group with a rigid backbone, (2) formation of a Fe–C(sp^2) bond and (3) forming a six-membered ring at Fe) implemented to disfavor alkyl migration from Fe to S upon oxidation. The numbering scheme corresponds to the clusters synthesized with the corresponding ligand.

3.2 Results and Discussion

2-methoxybenzyl magnesium bromide was used to prepare **4** (**Figure 3.2**); upon oxidation to the $[Fe_4S_4]^{3+}$ state, an $S = ½$ EPR signal with $g = [2.20, 2.03, 2.00]$ ($g_{avg} = 2.08$) was obtained (**Figure 3.3**). This signal was simulated with nearly the same parameters as the $S = ½$ signal for $[(IMes)_3Fe_4S_4(benzyl)]^{2+}$ (**10**), with $g = [2.22, 2.03, 1.99]$ ($g_{avg} = 2.08$), collected in a freeze-quench experiment in the absence of a coordinating solvent, suggesting that despite the presence of a methoxy oxygen atom, the Fe site remains tetrahedrally coordinated in the $[Fe_4S_4]^{3+}$ state.

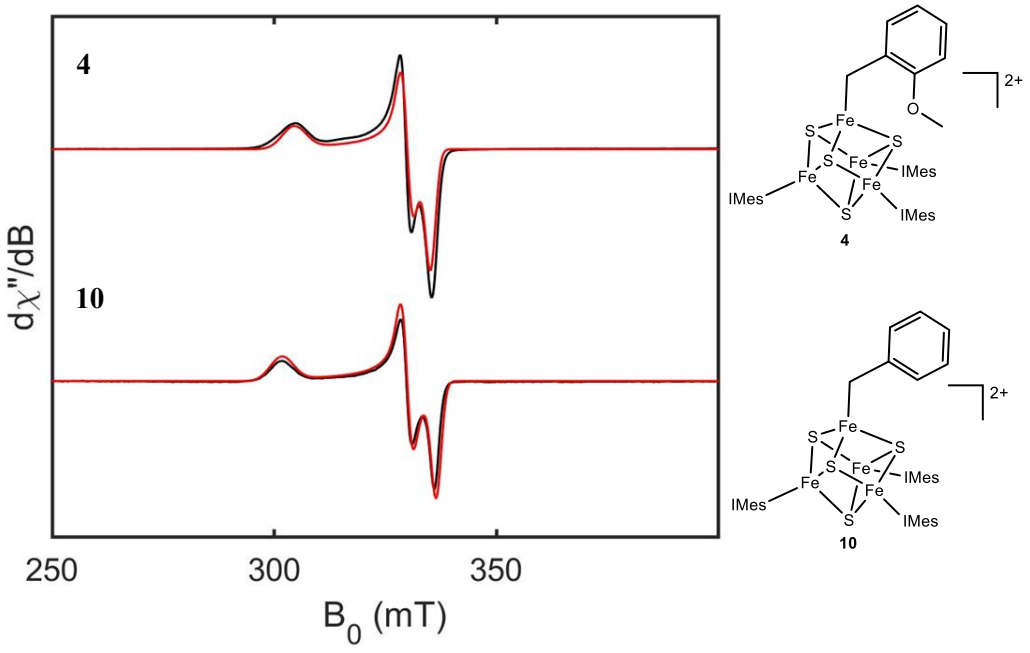

Figure 3.3 EPR signals of $[4]^{2+}$ (top) and $[(IMes)_3Fe_4S_4(benzyl)]^{2+}$ (bottom) at 15K and 63 μW. Black traces are experimental data and red traces are simulations. Simulation parameters for $[4]^{2+}$ are $g = [2.20, 2.03, 2.00]$ ($g_{avg} = 2.08$) and g-strain = [0.0445, 0.0150, 0.0144]. Simulation parameters for $[(IMes)_3Fe_4S_4(benzyl)]^{2+}$ are $g = [2.22, 2.03, 1.99]$ ($g_{avg} = 2.08$) and g-strain = [0.0445, 0.0150, 0.0144].

This result suggested that incorporation of a benzyl backbone disfavors alkyl migration from Fe to S upon oxidation. However, a stronger L-type donor could promote formation of a five-coordinate unique Fe site. Therefore, **5**, featuring an amine donor, was prepared and oxidized to the $[Fe_4S_4]^{3+}$ state. The EPR spectrum of $[\mathbf{5}]^{2+}$ contains two signals with $g_{eff} = 5.18$ and $g = [2.21, 2.01, 1.86]$, (**Figure S3.12**), which is consistent with that of $[\mathbf{1\text{-}MP}]^{2+}$ (**Figure 3.1**), with noninterconverting $S = 1/2$ and 7/2 spin systems. Likewise, the NMR spectrum of $[\mathbf{6}]^{2+}$, (**Figure S3.7**), which also contains an amine, L-type donor, features characteristically broad resonances at -1.39, 4.78 and 9.65 ppm, consistent with the S-alkylated species $[\mathbf{1\text{-}MP}]^{2+}$, and paramagnetically shifted resonances at -6.79 and 18.90 ppm that are unique to $[\mathbf{6}]^{2+}$. We therefore conclude that for benzyl-ligated clusters, a dangling amine appears to favor alkyl migration, unlike a dangling methoxy group, which does not coordinate the unique Fe.

Two-electron oxidation of the phenyl ligated clusters **7**, **8** and **9** from the $[Fe_4S_4]^+$ to the $[Fe_4S_4]^{3+}$ state results in alkyl migration from Fe to S regardless of the identity of the L-type donor or intended ring size at Fe. This is evidenced not only by the broad ^{1}H NMR resonances in their spectra (**Figure S3.8**, **Figure S3.9**, **Figure S3.10**) but also by the $S = 7/2$ signal in their EPR spectra with $g = \sim 5.18$ (**Figure S3.13**, **Figure S3.14**, **Figure S3.15**). Attempts to crystallize these species as $[B(C_6F_5)_4]^-$ salts by layering pentane onto a solution of *o*-difluorobenzene and storing at -35 °C, unfortunately, proved unsuccessful.

Despite efforts to purify these Fe-alkylated $[Fe_4S_4]^+$ and S-alkylated $[Fe_4S_4]^{3+}$ clusters, some samples contain, unidentified impurities (e.g., **Figure S3.4**, **Figure S3.10**, etc.). However, our confidence in the identification of these compounds remains high, as evidenced by the NMR and EPR spectra. In the case of Fe-alkylated $[Fe_4S_4]^+$ clusters, the NMR assignments and integrations were consistent with our expectations[2] and, although some samples were not of high purity, our oxidation experiments proved useful in assessing if they were a useful synthetic target (i.e., formation of a higher coordinate, alkylated Fe site). In the case of S-alkylated $[Fe_4S_4]^{3+}$ clusters, the impurities present are largely due to cluster degradation. This is consistent with the reported $[\mathbf{1\text{-}MP}]^{2+}$, which decomposes in solution at room temperature.[1] While the S-alkylated $[Fe_4S_4]^{3+}$ clusters are not pure, they meet the requirements for our research objective—to determine if specific ligand modifications would disfavor alkyl migration and enable us to isolate an $[Fe_4S_4]^{3+}$ cluster with a unique, five coordinate, alkylated Fe site. Upon oxidation of each of the clusters synthesized, excluding **4** (**Figure S3.11**), their NMR and EPR spectra are, as previously stated, most consistent with generation of S-alkylated $[Fe_4S_4]^{3+}$ clusters.[1]

These clusters are the first examples of benzyl and phenyl ligated, S-alkylated $[Fe_4S_4]^{3+}$ clusters. The occurrence of alkyl migration in these systems is further testament to the instability of alkyl-$[Fe_4S_4]^{3+}$ clusters and suggests that new approaches will be required to stabilize an oxidized cluster core. For example, replacement of N-heterocyclic carbene ligands by strongly electron donating ligands may enable isolation of oxidized clusters with unique, higher coordinate alkylated Fe sites.

3.3 Summary and Conclusions

The purpose of this work was to synthesize an alkyl-$[Fe_4S_4]^{3+}$ cluster containing a unique alkylated Fe site with a coordination number of five to serve as a model of proposed intermediates in radical reactions performed by $[Fe_4S_4]$ clusters. To achieve this, a series of benzyl and phenyl ligands containing an L-type donor atom were synthesized and bound to the unique Fe site of a 3:1 site differentiated $[Fe_4S_4]$ cluster. Results show that alkyl migration in benzyl ligated clusters is dependent upon the identity of the L-type donor atom; a 2-methoxybenzyl bound cluster does not form an S-alkylated species upon oxidation whereas the 2-dimethylaminobenzyl bound cluster did generate an S-alkylated species. In each phenyl ligated cluster synthesized, alkyl migration occurred upon oxidation to the $[Fe_4S_4]^{3+}$ state regardless of the L-type donor. These results highlight the challenges in stabilizing alkylated Fe sites within $[Fe_4S_4]^{3+}$ clusters. Further investigation is needed to stabilize an alkylated, five-coordinate unique Fe site effectively such as replacement of N-heterocyclic carbene ligands with strongly electron-donating groups to facilitate the isolation of oxidized clusters. These findings contribute to the understanding of alkyl-$[Fe_4S_4]^{3+}$ cluster stability and suggest avenues for further exploration.

3.4 Experimental

General Considerations. All reactions were performed using standard Schlenk techniques or in an LC Technologies inert-atmosphere glovebox under an atmosphere of dinitrogen. Glassware was dried in an oven at 160 °C prior to use. Molecular sieves (3 Å) and Celite were activated by heating to 300 °C overnight under vacuum prior to storage under an atmosphere of dinitrogen. Diethyl ether (Et_2O) and toluene were degassed by sparging with argon, dried by passing through a column of activated alumina and stored under an atmosphere of dinitrogen over 3 Å molecular sieves. o-Difluorobenzene (o-DFB) was distilled from CaH_2, C_6D_6 was degassed by three freeze-pump-thaw cycles. Tetrahydrofuran (THF) was distilled from sodium/benzophenone and stored under an atmosphere of dinitrogen over 3 Å molecular sieves. C_6D_6 was degassed by three freeze-pump-thaw cycles and stored under an atmosphere of dinitrogen over 3 Å molecular sieves. Grignard reagents were prepared by addition of the alkyl halide[4-22] to activated magnesium turnings in THF. [Fc][$BArF_4$] ([$BArF_4$] = [B(3,5-(CF_3)$_2$Ph)$_4$]) and (IMes)$_3$$Fe_4S_4$Cl (IMes = 1,3-dimesitylimidazol-2-ylidene) were synthesized by reported procedures.[3,4] All other reagents were purchased from commercial suppliers and used without further purification/drying unless otherwise noted. NMR spectra were recorded on Bruker 400 and 500 MHz spectrometers. EPR spectra were recorded on a Bruker EMX spectrometer at 9.37 GHz as frozen glasses.

General Preparation of Alkylated [Fe_4S_4] Clusters

A solution of Grignard reagent (0.1 M in THF, 1.05 equiv) was added dropwise to a solution of (IMes)$_3$$Fe_4S_4$Cl (1 equiv) in a 1:1 mixture of Et_2O and THF (1 mL). After 20 minutes the solution was diluted with copious Et_2O (600% of initial reaction volume) and 1,4-Dioxane (50% of initial reaction volume) was added with vigorous stirring. After 10 minutes, the solution was filtered through celite and the filtrate was reduced to dryness. The resulting precipitate was redissolved in copious Et_2O and 1,4-dioxane was added to the solution. After vigorous stirring for 30 minutes, the solution was filtered through celite and reduced to dryness.

(IMes)$_3$$Fe_4S_4$(2-methoxybenzyl) (4)

4 was isolated as a dark brown solid (67%). This sample contains unknown impurities from the Grignard reagent. ^{1}H NMR (400 MHz, C_6D_6, 298 K): δ 225 (s, 2H, FeCH_2), 11.45 (s, 1H, benzyl *m*-C*H*), 10.79 (s, 1H, benzyl *m*-C*H*), 6.98 (s, 12H, IMes Ar*H*), 5.94 (s, 6H, backbone C*H*), 2.35 (s, 18H, Mes *p*-CH_3), 2.00 (s, 36H, Mes *o*-CH_3), -5.44 (s, 1H, benzyl *o*-C*H*), -7.01 (s, 1H, benzyl *p*-C*H*).

(IMes)$_3$$Fe_4S_4$(2-dimethylaminobenzyl) (5)

5 was isolated as a dark brown solid (68%). This sample contains unknown impurities. ^{1}H NMR (400 MHz, C_6D_6, 298 K): δ 226 (s, 2H, Fe CH_2), 11.21 (s, 1H, benzyl *m*-C*H*), 11.11 (s, 1H, benzyl *m*-C*H*), 6.97 (s, 12H, IMes Ar*H*), 5.93 (s, 6H, backbone C*H*), 2.34 (s, 18H, Mes *p*-CH_3), 2.02 (s, 36H, Mes *o*-CH_3), -3.96 (s, 1H, benzyl *o*-C*H*), -5.02 (s, 1H, benzyl *p*-C*H*).

(IMes)$_3$$Fe_4S_4$(2-dimethylaminomethylbenzyl) (6)

6 was isolated as a dark brown solid (61%). This sample contains unknown impurities from the Grignard reagent. ^{1}H NMR (400 MHz, C_6D_6, 298 K): δ 226 (s, 2H, FeCH_2), 11.47 (s, 1H, benzy *m*-C*H*), 11.31 (s, 1H, benzyl *m*-C*H*), 10.3 (s, 2H, CH_2NMe_2), 7.01 (s, 12H, IMes Ar*H*), 5.92 (s,

6H, backbone C*H*), 2.36 (s, 18H, Mes *p*-CH_3), 2.02 (s, 36H, Mes *o*-CH_3), -3.24 (s, 1H, benzyl *o*-C*H*), -6.02 (s, 1H, benzyl *p*-C*H*).

(IMes)$_3$Fe$_4$S$_4$(2-methoxymethylphenyl) (7)

7 was isolated as a dark red, brown solid (56%). This sample contains unknown impurities. ^{1}H NMR (400 MHz, C_6D_6, 298 K): δ 25.78 (s, 1H, phenyl *m*-C*H*), 25.06 (s, 1H, phenyl *m*-C*H*), 14.08 (s, 1H, phenyl *o*-C*H*), 6.97 (s, 12H, IMes Ar*H*), 6.01 (s, 6H, backbone C*H*), 2.27 (s, 18H, Mes *p*-CH_3), 2.18 (s, 36H, Mes *o*-CH_3), -9.33 (s, 1H, phenyl *p*-C*H*).

(IMes)$_3$Fe$_4$S$_4$(2-dimethylaminomethylphenyl) (8)

8 was isolated as a dark red, brown solid (55%). This sample contains unknown impurities. ^{1}H NMR (400 MHz, C_6D_6, 298 K): δ 25.49 (s, 1H, phenyl *m*-C*H*), 23.90 (s, 1H, phenyl *m*-C*H*), 15.83 (s, 1H, phenyl *o*-C*H*), 13.68 (s, 2H, CH_2NMe$_2$), 6.98 (s, 12H, IMes Ar*H*), 6.05 (s, 6H, backbone C*H*), 2.30 (s, 18H, Mes *p*-CH_3), 2.16 (s, 36H, Mes *o*-CH_3), -8.48 (s, 1H, phenyl *p*-C*H*).

(IMes)$_3$Fe$_4$S$_4$(2-methoxyethylphenyl) (9)

9 was isolated as a dark brown solid (32%). This sample contains unknown impurities. ^{1}H NMR (400 MHz, C_6D_6, 298 K): δ 25.51 (s, 1H, phenyl *m*-C*H*), 24.63 (s, 1H, phenyl *m*-C*H*), 15.10 (s, 1H, phenyl *o*-C*H*), 10.13 (s, 2H, CH_2CH$_2$OMe), 7.01 (s, 12H, IMes Ar*H*), 6.02 (s, 6H, backbone C*H*), 2.29 (s, 18H, Mes *p*-CH_3), 2.19 (s, 36H, Mes *o*-CH_3), -9.18 (s, 1H, phenyl *p*-C*H*).

General Method of Oxidation of Alkylated [Fe$_4$S$_4$] clusters

The alkylated cluster (1 equiv) and [Fc][BArF$_4$] (1.05 equiv) were separately dissolved in an 9:1 mixture of o-DFB and toluene (0.9 mL each) and cooled to -35 °C. The solution of [Fc][BArF$_4$] was added to the (IMes)$_3$Fe$_4$S$_4$(CH$_2$CH$_3$) solution and immediately an aliquot of the reaction mixture (0.2 mL) was transferred into an X-band EPR tube and glassed in liquid nitrogen. Due to its thermal instability, this compound was made freshly for all experiments.

[(IMes)$_3$Fe$_4$S$_4$(2-dimethylaminomethylbenzyl)][BArF]$_2$ ([6]$^{2+}$)

[6]$^{2+}$ was isolated as a brown, black oily solid (40%). This sample contains an unknown decomposition product. ^{1}H NMR (400 MHz, o-DFB, 298K): δ 18.90, 9.65, 8.05, 7.40, 4.87, -1.39, -6.79 (assignments were not made because of the broadness of the peaks).

[(IMes)$_3$Fe$_4$S$_4$(2-methoxymethylphenyl)][BArF]$_2$ ([7]$^{2+}$)

[7]$^{2+}$ was isolated as a purple, black oily solid (37%). This sample contains an unknown decomposition product. ^{1}H NMR (400 MHz, o-DFB, 298K): δ 88.37, 85.58, 11.28, 8.48, 7.47, 4.50, -2.35, -88.27 (assignments were not made because of the broadness of the peaks).

[(IMes)$_3$Fe$_4$S$_4$(2-dimethylaminomethylphenyl)][BArF]$_2$ ([8]$^{2+}$)

[8]$^{2+}$ was isolated as a purple, black oily solid (30%). This sample contains an unknown decomposition product. ^{1}H NMR (400 MHz, o-DFB, 298K): δ 90.82, 84.52, 10.66, 8.18, 7.56, 5.82, 4.56, -1.97, -91.25 (assignments were not made because of the broadness of the peaks).

[(IMes)$_3$Fe$_4$S$_4$(2-methoxyethylphenyl)][BArF]$_2$ ([9]$^{2+}$)

[9]$^{2+}$ was isolated as a purple, black oily solid (22%). This sample contains an unknown decomposition product and unidentified impurities. ^{1}H NMR (400 MHz, o-DFB, 298K): δ 91.80, 83.40, 9.26, 8.09, 7.45, 5.73, -2.55, -80.57 (assignments were not made because of the broadness of the peaks).

3.5 References

(1) Ye, M.; Brown, A. C.; Suess, D. L. M. Reversible Alkyl-Group Migration between Iron and Sulfur in [Fe_4S_4] Clusters. *J. Am. Chem. Soc.* **2022**, *144* (29), 13184–13195.

(2) Brown, A. C.; Suess, D. L. M. Reversible Formation of Alkyl Radicals at [Fe_4S_4] Clusters and Its Implications for Selectivity in Radical SAM Enzymes. *J. Am. Chem. Soc.* **2020**, *142* (33), 14240–14248.

(3) Brown, A. C.; Suess, D. L. M. Controlling Substrate Binding to [Fe_4S_4] Clusters through Remote Steric Effects. *Inorg. Chem.* **2019**, *58* (8), 5273–5280.

(4) Blechschmidt, D. R.; Lovstedt, A.; Kass, S. R. Metallocenium Lewis Acid Catalysis for Use in Friedel-Crafts Alkylation and Diels-Alder Reactions. *Organometallics*. **2022**, *41*(18), 2648-2655

(5) Lian, F.; Sun, C.; Xu, K.; Zeng, C. Electrochemical Dehydrogenative Imidation of N-Methyl-Substituted Benzylamines with Phthalimides for the Direct Synthesis of Phthalimide-Protected gem-Diamines. *Org. Lett.* **2019**, 21, 1, 156-159

(6) Ludt, R. E.; Crowther, G. P.; Hauser, C. R. The Effect of Tetramethylethylenediamine on the Metalation of *o*-and *p*-N,N-Dimethyltoluidines with *n*-Butyllithium. Deuteration and Electrophilic Condensation of Intermediate Lithioamines. *J. Org. Chem.* **1970**, 35, 5, 1288-1296

(7) Vaulx, R. L.; Jones, F. N.; Hauser, C. R. Condensations of 2-Dimethylaminomethylbenzyllithium and Related Amino Organolithium Reagents with Aldehydes and Ketones. Cyclizations to Isochromans. *J. Org. Chem.* **1964**, 29, 1387-1391

(8) Kim, E. H.; Lee, H. M.; Jeong, M. S.; Ryu, J. Y.; Lee, J.; Lee, B. Y. Methylaluminoxane-Free Chromium Catalytic System for Ethylene Tetramerization. *ACS Omega*. **2017**, 2, 3, 765-773

(9) Allan, K. M.; Spencer, J. L. The synthesis and characterisation of novel o-substituted benzyldi-t-butylphosphine–boranes. *Tetrahedron Lett.* **2009**, 50, 7, 834-835

(10) Bisht, R.; Hoque, M. E.; Chattopadhyay, B. Amide Effects in C−H Activation: Noncovalent Interactions with L-Shaped Ligand for meta Borylation of Aromatic Amides. *Angew. Chem. Int. Ed.* **2018**, 57, 15762

(11) Lu, X.; Yoshigoe, Y.; Ida, H.; Nishi, M.; Kanai, M.; Kuninobu, Y. Hydrogen Bond-Accelerated meta-Selective C–H Borylation of Aromatic Compounds and Expression of Functional Group and Substrate Specificities. *ACS Catal.* **2019**, 9, 3, 1705-1709

(12) Gómez-Santacana, X.; de Munnik, S. M.; Vijayachandran, P.; Da Costa Pereira, D.; Bebelman, J. P. M.; de Esch, I. J. P.; Vischer, H. F.; Wijtmans, M.; Leurs, R. Photoswitching the Efficacy of a Small-Molecule Ligand for a Peptidergic GPCR: from Antagonism to Agonism. *Angew. Chem. Int. Ed.* **2018**, 57, 11608

(13) Ŝkalamera, D.; Bregović, V. B.; Antol, I.; Bohne, C.; Basarić, N. Hydroxymethylaniline Photocages for Carboxylic Acids and Alcohols. *J. Org. Chem.* **2017**, 82, 23, 12554-12568

(14) Hedberg, C.; Jessen, K. S.; Hansson, R. F.; Heuckendorff, M.; Jensen, H. H. Palladium-Catalyzed C–S Bond Formation as a Tool for Latent–Active Glycosylation. *Org. Lett.* **2020**, 22, 18, 7068-7072

(15) Smith, D. J.; Yap, G. P. A.; Kelley, J. A.; Schneider, J. P. Enhanced Stereoselectivity of a Cu(II) Complex Chiral Auxiliary in the Synthesis of Fmoc-l-γ-carboxyglutamic Acid. *J. Org. Chem.* **2011**, 76, 6, 1513-1520

(16) Ding, Z.-Y.; Wang, T.; He, Y.-M.; Chen, F.; Zhou, H.-F.; Fan, Q.-H.; Guo, Q.; Chan, A. S. C. Highly Enantioselective Synthesis of Chiral Tetrahydroquinolines and Tetrahydroisoquinolines by Ruthenium-Catalyzed Asymmetric Hydrogenation in Ionic Liquid. *Adv. Synth. Catal.* **2013**, 355, 18, 3727-3735.

(17) Lin, H.-S.; Jeon, I.; Chen, Y.; Yang, X.-Y.; Nakagawa, T.; Maruyama, S.; Manzhos, S.; Matsuo, Y. Highly Selective and Scalable Fullerene-Cation-Mediated Synthesis Accessing Cyclo[60]fullerenes with Five-Membered Carbon Ring and Their Application to Perovskite Solar Cells. *Chem. Mater.* **2019**, 31, 20, 8432-8439

(18) Kobin, B.; Bianchi, F.; Halm, S.; Leistner, J.; Blumstengel, S.; Henneberger, F.; Hecht, S. Green Emission in Ladder-Type Quarterphenyl: Beyond the Fluorenone-Defect. *Adv. Funct. Mater.*, **2014**, 24, 48, 7717-7727.

(19) Zhang, X.; Sivaguru, P.; Zanoni, G.; Han, X.; Tong, M.; Bi, X. Catalytic Asymmetric C(sp^3)–H Carbene Insertion Approach to Access Enantioenriched 3-Fluoroalkyl 2,3-Dihydrobenzofurans. *ACS Catal.* **2021**, 11, 22, 14293-14301

(20) Yang, X.-Y.; Lin, H.-S.; Matsuo, Y. Highly Selective Synthesis of Tetrahydronaphthaleno[60]fullerenes via Fullerene-Cation-Mediated Intramolecular Cyclization. *J. Org. Chem.* **2019**, 84, 24, 16314-16322

(21) Doan, T.-H.; Chardon, A.; Osi, A.; Mahaut, D.; Tumanov, N.; Wouters, J.; Champagne, B.; Berionni, C. Methylene Bridging Effect on the Structures, Lewis Acidities and Optical Properties of Semi-planar Triarylboranes. *Chem. Eur. J.* **2021**, 27, 5, 1736-1743

(22) Mihai, M. T.; Davis, H. J.; Genov, G. R.; Phipps, R. J. Ion Pair-Directed C–H Activation on Flexible Ammonium Salts: meta-Selective Borylation of Quaternized Phenethylamines and Phenylpropylamines. *ACS Catal.* **2018**, 8, 5, 3764-3769

3.6 Spectra

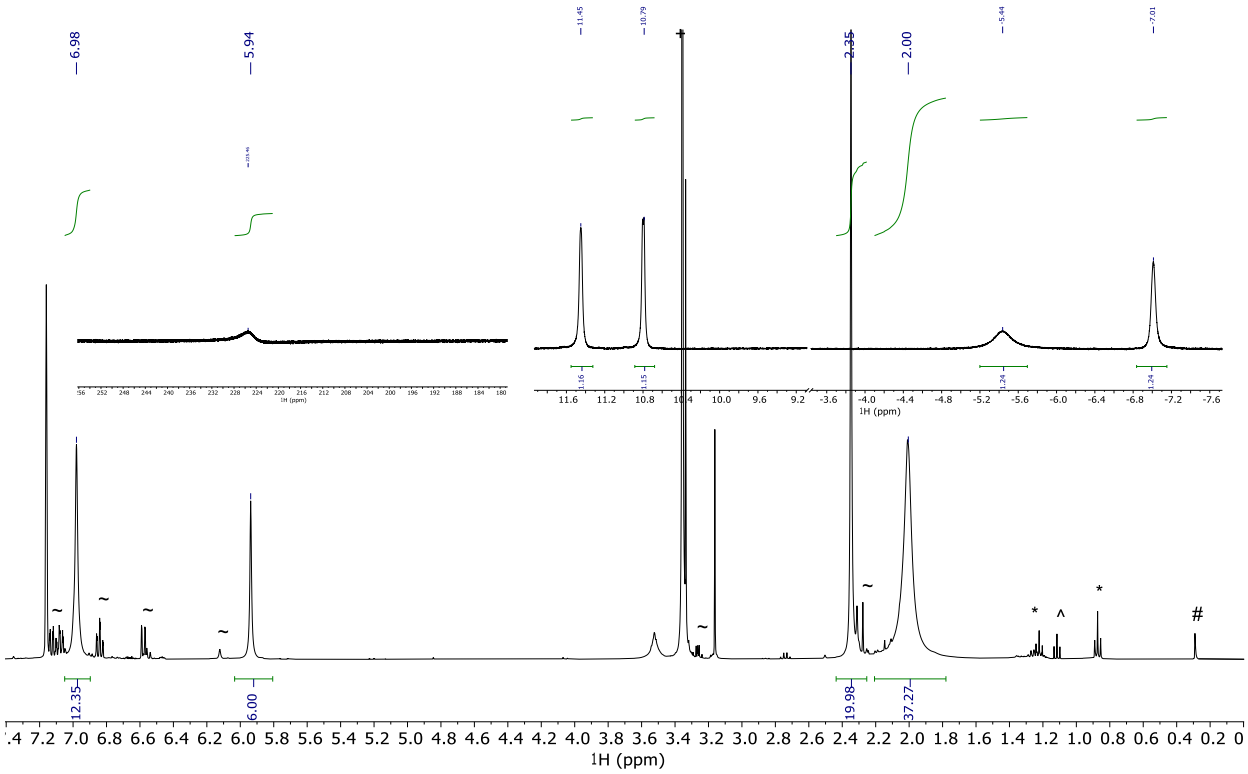

Figure S3.1. ^{1}H-NMR spectrum of $(IMes)_3Fe_4S_4$(2-methoxybenzyl) (**4**) in C_6D_6 (* pentane, ^ Et_2O, # grease, + dioxane, ~impurities from Grignard)

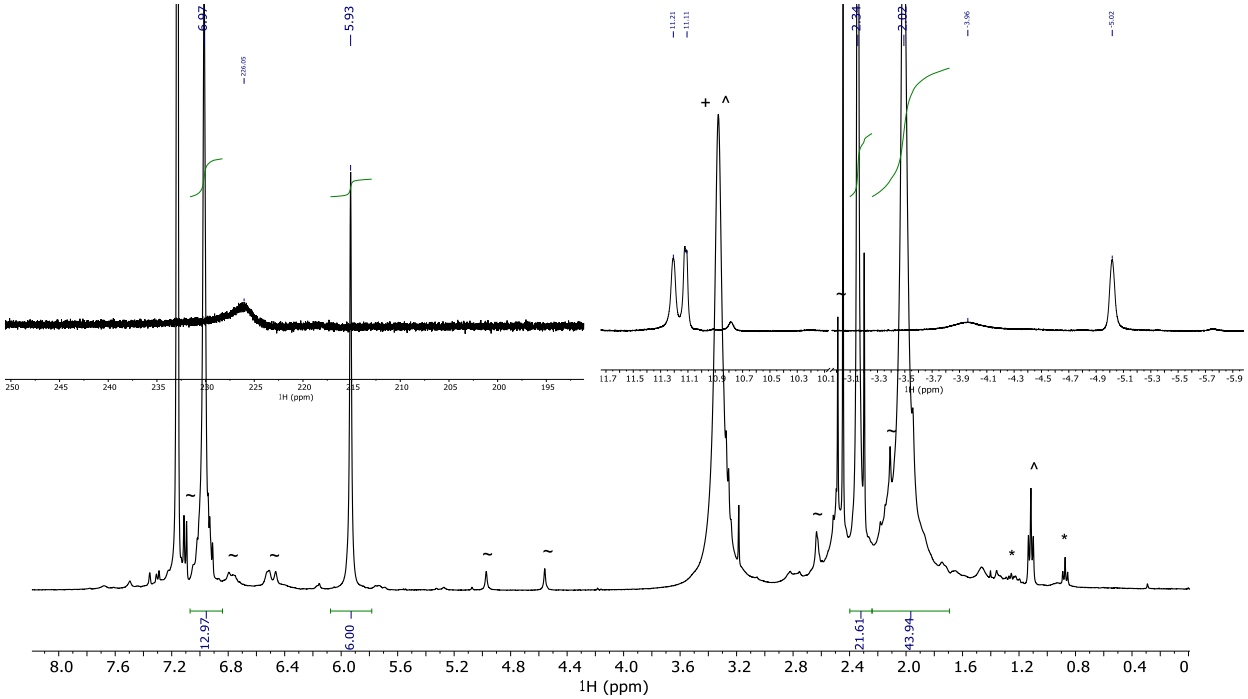

Figure S3.2. ^{1}H-NMR spectrum of $(IMes)_3Fe_4S_4$(2-dimethylaminobenzyl) (**5**) in C_6D_6 (*pentane, ^ Et_2O, ~ unidentified impurities, +dioxane)

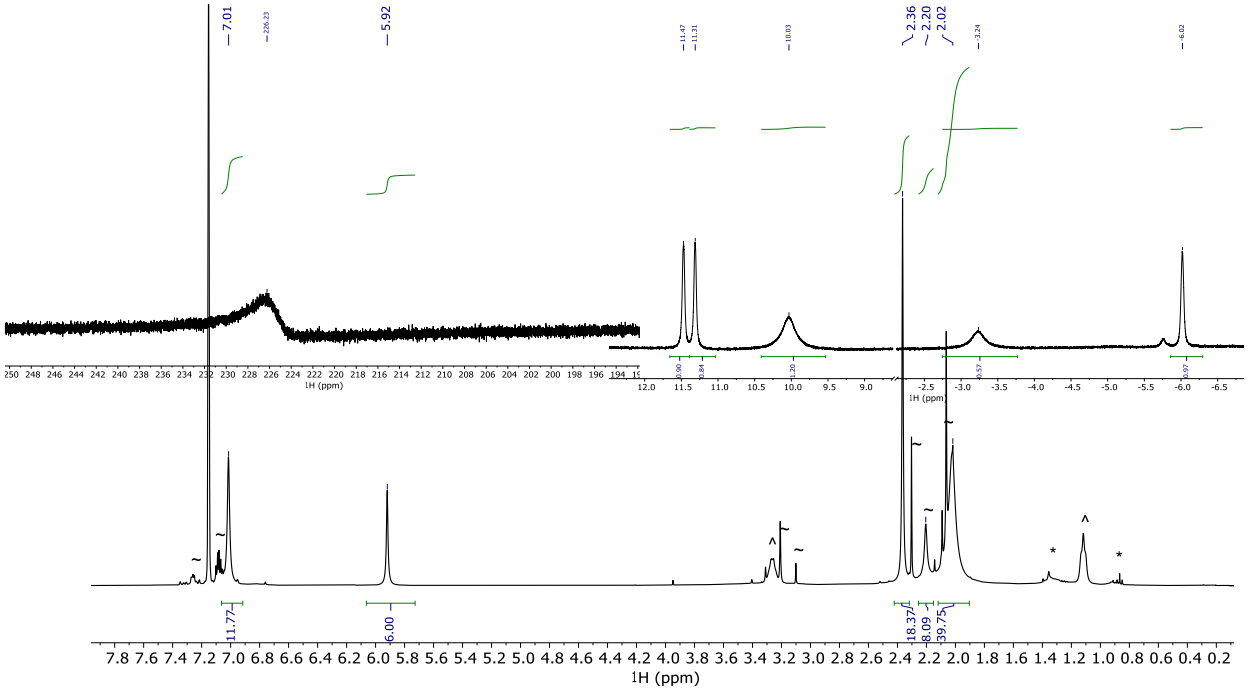

Figure S3.3. ^{1}H-NMR spectrum of $(IMes)_3Fe_4S_4$(2-dimethylaminomethylbenzyl) (**6**) in C_6D_6 (*pentane, ^ Et_2O, ~ impurities from Grignard)

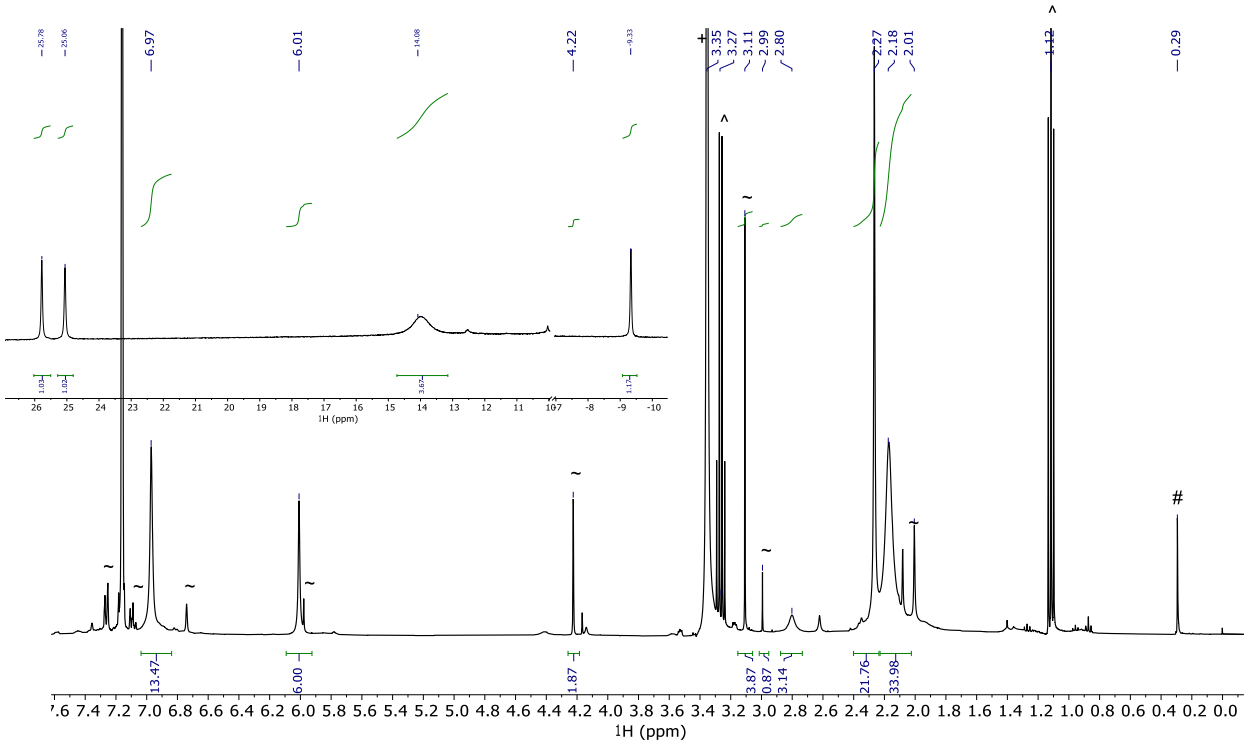

Figure S3.4. ^{1}H-NMR spectrum of $(IMes)_3Fe_4S_4$(2-methoxymethylphenyl) (**7**) in C_6D_6 (^ Et_2O, # grease, ~ unknown impurities)

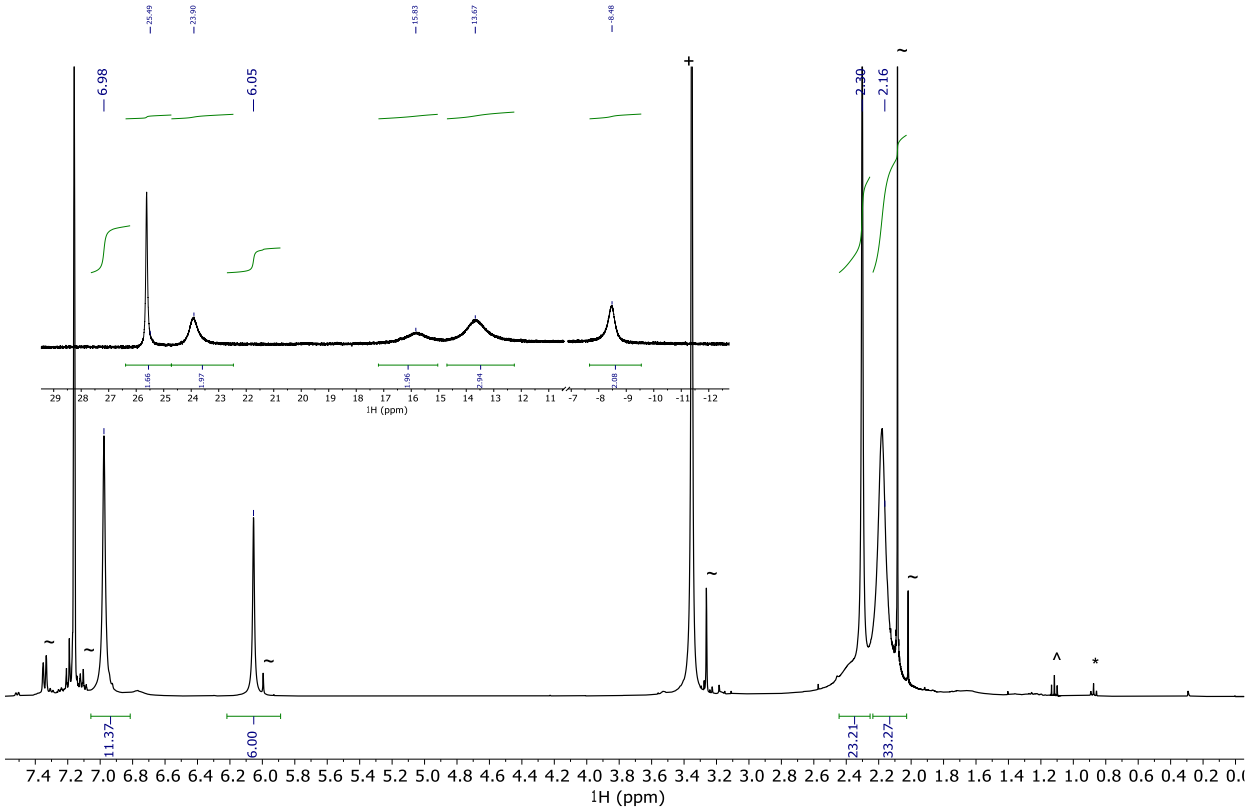

Figure S3.5. ^{1}H-NMR spectrum of $(IMes)_3Fe_4S_4$(2-dimethylaminomethylphenyl) (**8**) in C_6D_6 (* pentane, ^Et_2O, + dioxane, ~ unknown impurities)

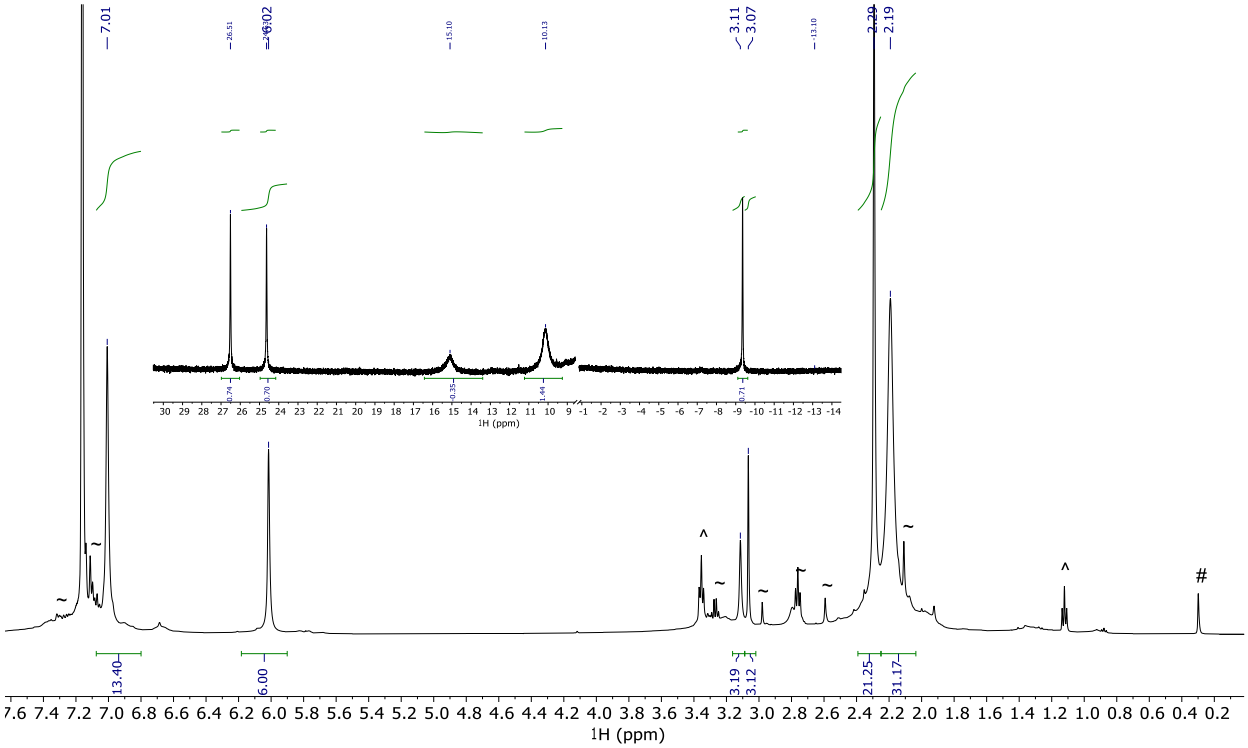

Figure S3.6. ^{1}H-NMR spectrum of $(IMes)_3Fe_4S_4$(2-methoxyethylphenyl) (**9**) in C_6D_6 (^ Et_2O, # grease, ~ unknown impurities)

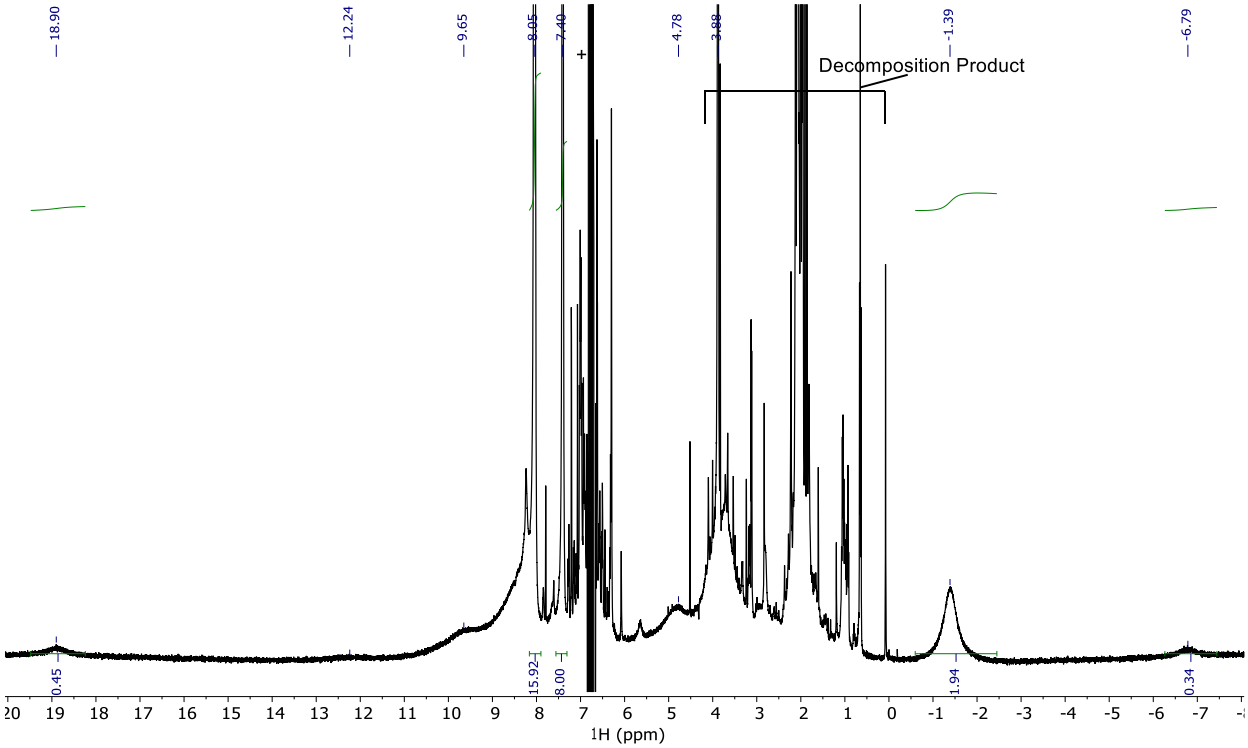

Figure S3.7. ^{1}H-NMR spectrum of $[(IMes)_3Fe_4S_4(2\text{-dimethylaminomethylbenzyl})][BArF]_2$ (**[6]**$^{2+}$) in o-DFB (+ o-DFB)

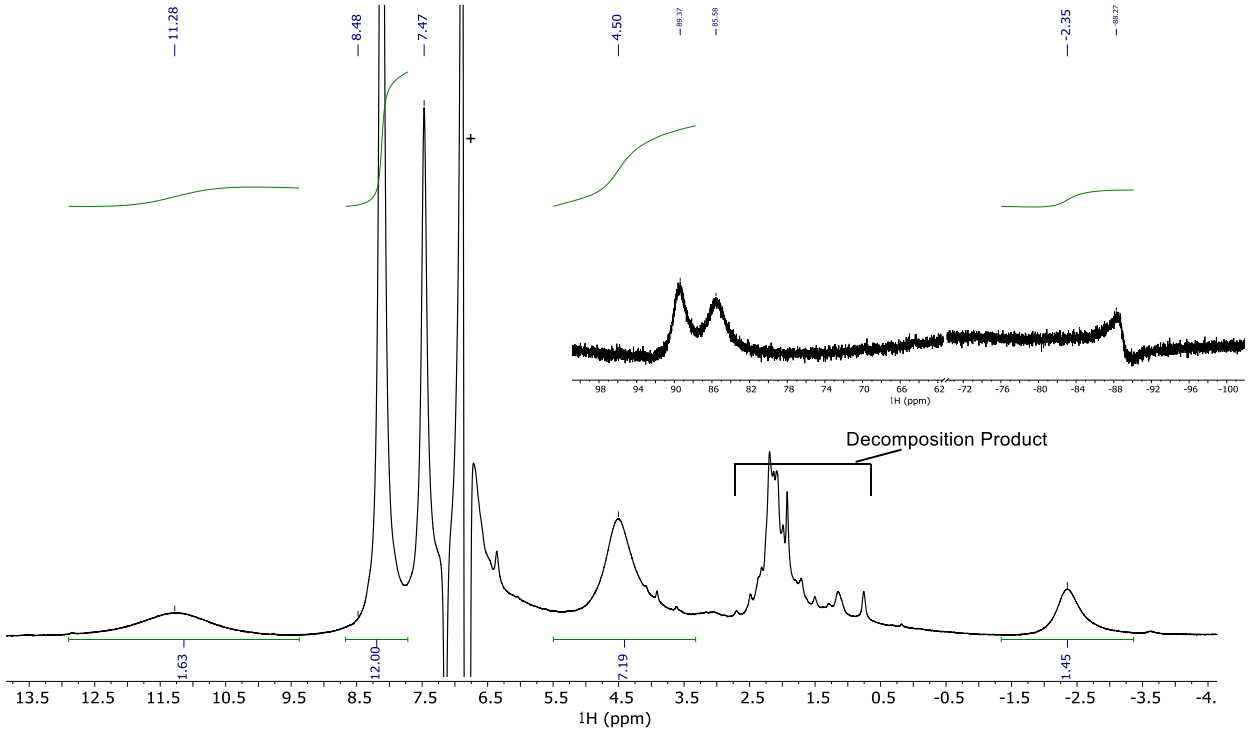

Figure S3.8. ^{1}H-NMR spectrum of [(IMes)$_3$Fe$_4$S$_4$(2-methoxymethylphenyl)][BArF]$_2$ **[7]$^{2+}$**)in o-DFB (+ o-DFB)

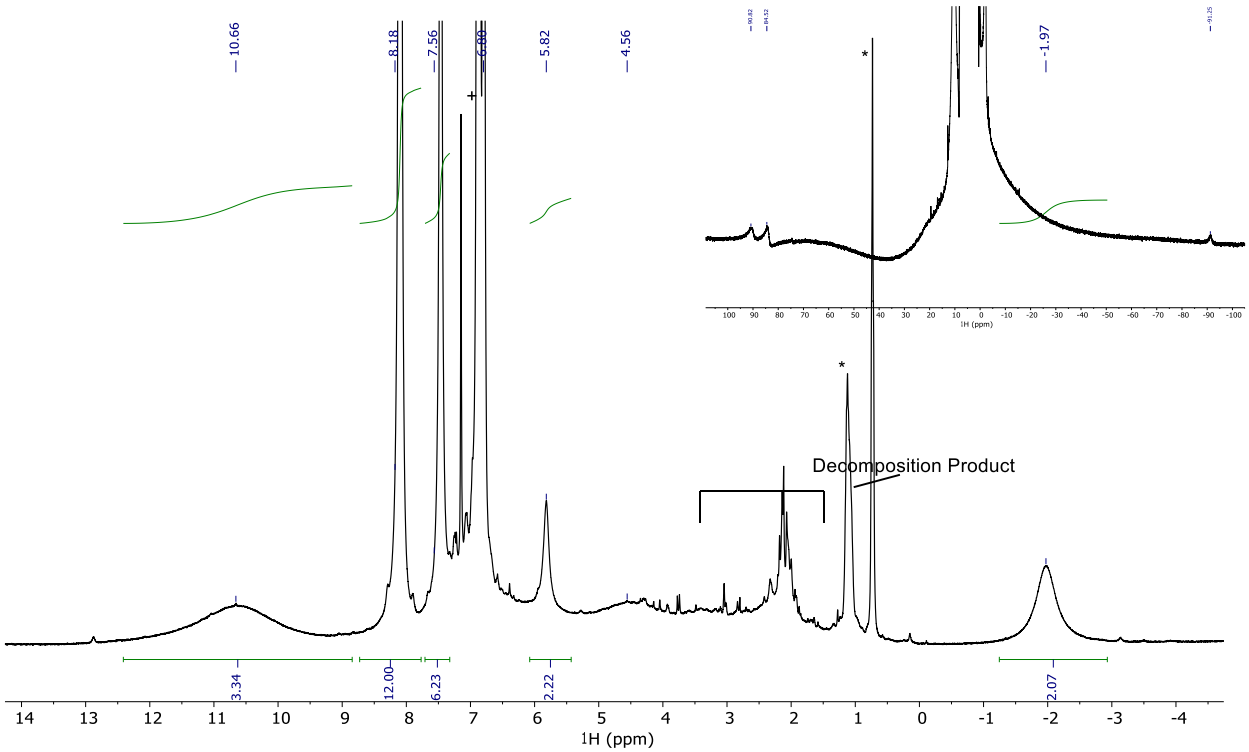

Figure S3.9. ^{1}H-NMR spectrum of [(IMes)$_3$Fe$_4$S$_4$(2-dimethylaminomethylphenyl)][BArF]$_2$ **[8]**$^{2+}$)in o-DFB (+o-DFB, *hexanes)

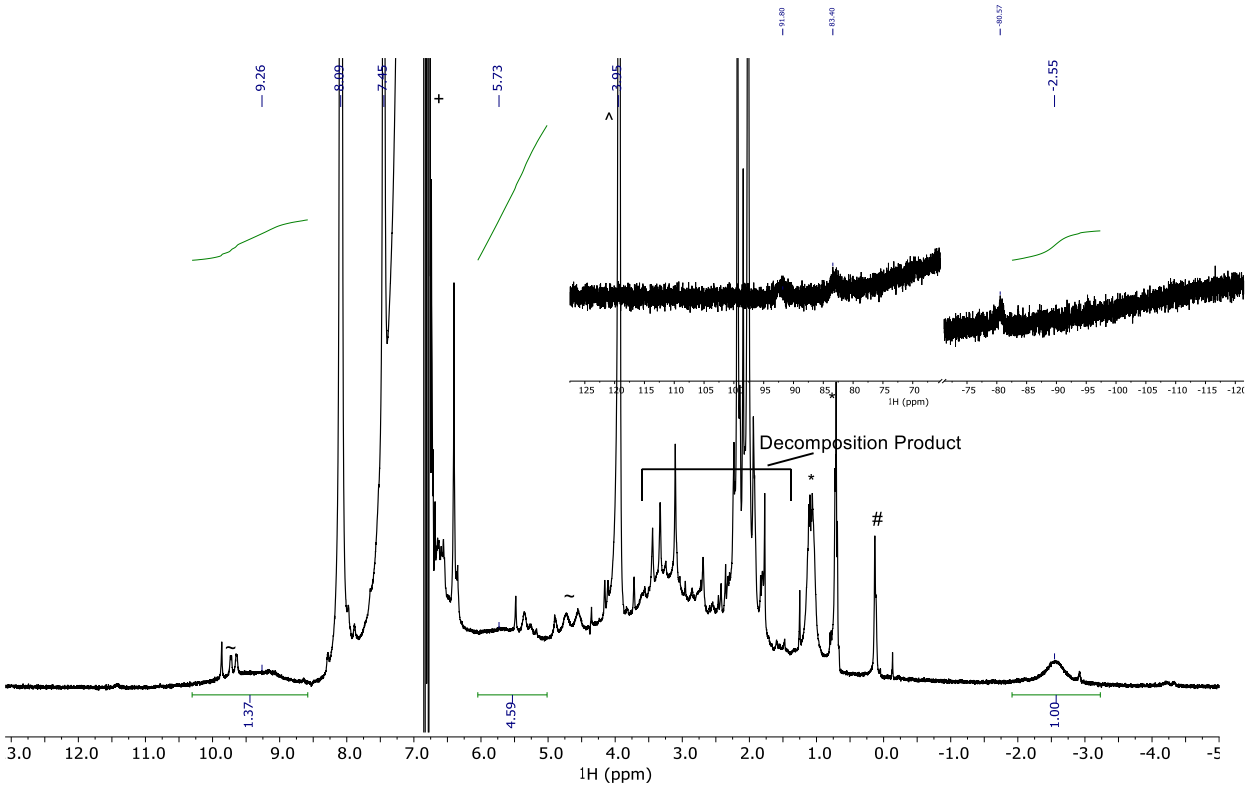

Figure S3.10. ^{1}H-NMR spectrum of $[(IMes)_3Fe_4S_4(2\text{-methoxyethylphenyl})][BArF]_2$ **[9]**$^{2+}$)in o-DFB (+o-DFB, * pentane, # grease, ^ferrocene, ~ unknown impurities)

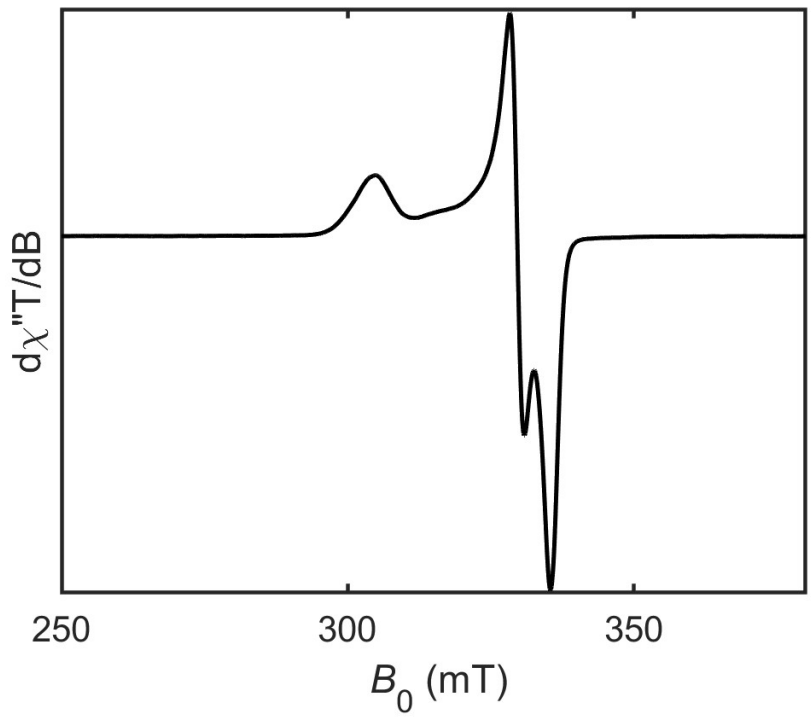

Figure S3.11. X-band EPR spectrum of $[(IMes)_3Fe_4S_4(2\text{-methoxybenzyl})][BArF]_2$ ($\mathbf{[4]^{2+}}$)(g = [2.20, 2.03, 2.00], 15K, 63μW)

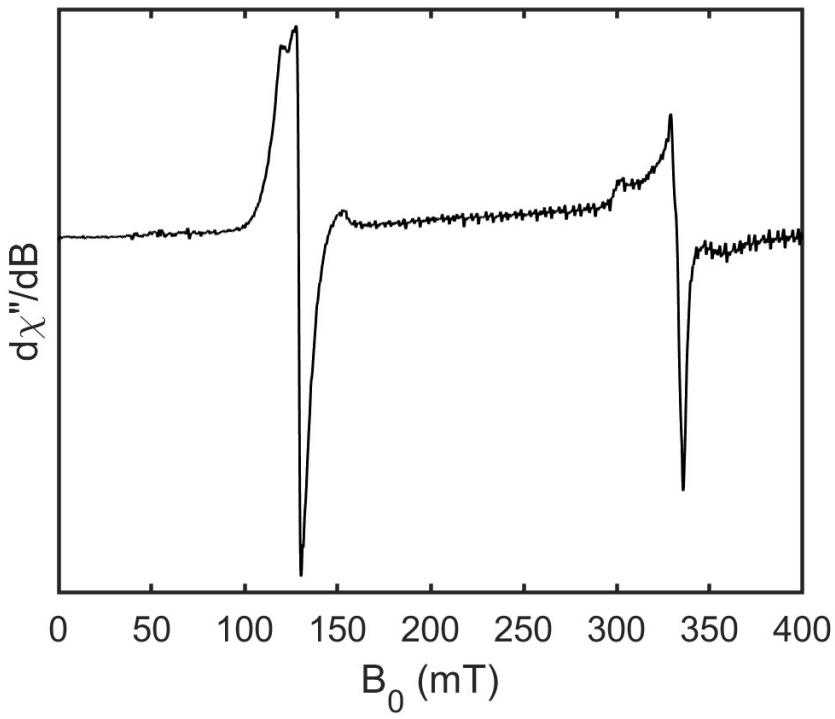

Figure S3.12. X-band EPR spectrum of $[(IMes)_3Fe_4S_4(2\text{-dimethylaminobenzyl})][BArF]_2$ (**[5]**$^{2+}$)(features at g_{eff} = 5.18 for the S = 7/2 signal and g = [2.21, 2.01,1.86] for the S = 1/2 signal, 15K, 63μW)

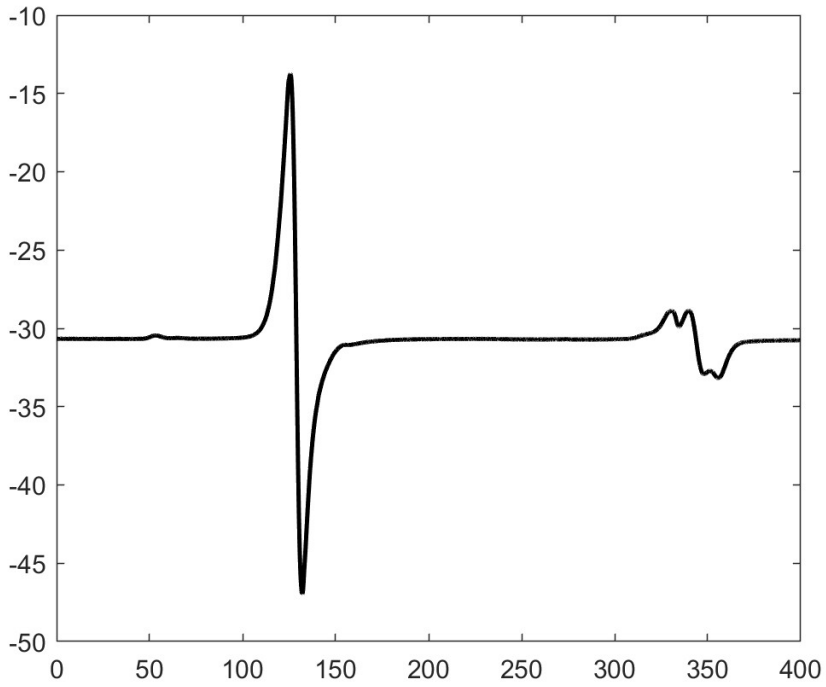

Figure S3.13. X-band EPR spectrum of $[(IMes)_3Fe_4S_4(2\text{-methoxymethylphenyl})][BArF]_2$ (**[7]**$^{2+}$)(features at g_{eff} = 12.56 and 5.18 for the S = 7/2 signal and g = [2.03, 1.94, 1.88] for the S = 1/2 signal, 15K, 63μW)

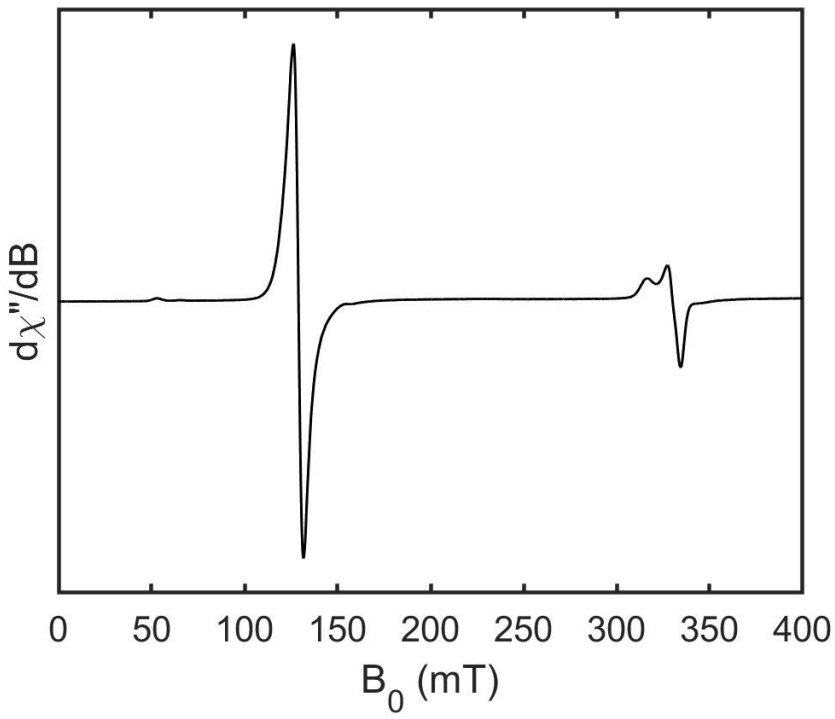

Figure S3.14. X-band EPR spectrum of $[(IMes)_3Fe_4S_4(2\text{-dimethylaminomethylphenyl})][BArF]_2$ (**[8]**$^{2+}$)(features at g_{eff} = 12.4 and 5.18 for the S = 7/2 signal and g = [2.12, 2.12, 2.02] for the S = 1/2 signal, 15K, 63μW)

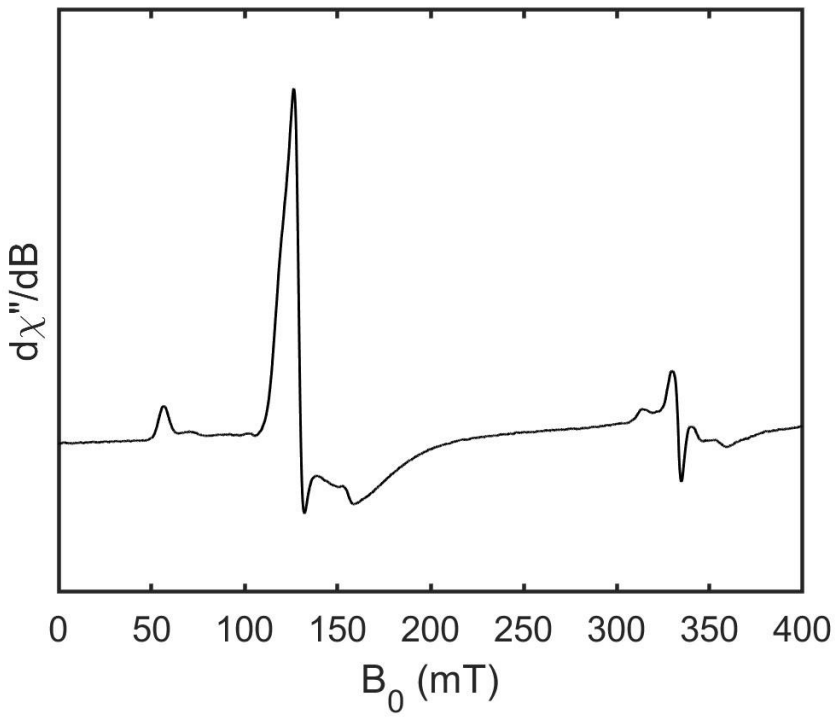

Figure S3.15. X-band EPR spectrum of $[(IMes)_3Fe_4S_4(2\text{-methoxyethylphenyl})][BArF]_2$ (**[9]**$^{2+}$)(features at g_{eff} = 11.6 and 5.17 for the S = 7/2 signal and g = [2.15, 2.01, 1.88] for the S = 1/2 signal, 15K, 63μW)